https://doi.org/10.1016/j.jaerosci.2015.05.011

A bimodal moment method model for submicron fractal-like agglomerates undergoing Brownian coagulation

Mingzhou Yu [a,b] and Tat Leung Chan[b*]

[a]*China Jiliang University, Hangzhou, 310018, People's Republic of China*

[b]*Department of Mechanical Engineering, The Hong Kong Polytechnic University, Hung Hom, Kowloon, Hong Kong*

[*]Corresponding Author: Tat Leung Chan, Department of Mechanical Engineering, The Hong Kong Polytechnic University, Kowloon, Hong Kong. E-mail: mmtlchan@polyu.edu.hk

Abstract

A new bimodal moment method for submicron fractal-like agglomerates undergoing Brownian coagulation is developed. The entire bimodal agglomerate size distribution is firstly separated into two separated distributions, where each distribution is represented by a population balance equation. The two joint population balance equations are then resolved by introducing the Taylor expansion method of moments (TEMOM). This newly developed bimodal model (B-TEMOM) is compared with the commonly used bimodal log-normal method of moments (B-log MM), and bimodal quadrature method of moments (B-QMOM) for the first three moments as well as geometric standard deviation of number distribution. Compared to the B-QMOM, the solution suggests that the B-TEMOM and the B-log MM produce much closer results. With the increase in the difference of the total particle number concentration, the geometric standard deviation, and the geometric mean volume of two modes, the difference among the investigated bimodal models is also slightly increased. The difference between B-log MM and B-TEMOM is found to increase with a decrease in mass fractal dimension, especially at a later stage in the evolution. The solution fully verifies that this newly developed B-TEMOM is reliable for predicting agglomerate dynamics undergoing Brownian coagulation in the continuum-slip regime.

Keywords: Bimodal moment method model scheme; Population balance equation; Submicron fractal-like agglomerate; Brownian coagulation.

Nomenclature

A	constant (= 1.591)
d	particle diameter, m
n, p	particle number concentration density , m^{-3}
B_2	collision coefficient for the continuum-slip regime
C	Cunningham correction factor
k_B	Boltzmann constant, J·K
Kn	particle Knudsen number
m_k	kth moment of particle size distribution
M_k	dimensionless kth moment of size distribution
t	time, s
T	temperature, K
U	the point of Taylor-series expansion (m_1/m_0)
v	particle volume, m^3
v_g	geometric mean particle volume, m^3
N	initial total particle number concentration, m^{-3}
D_f	Mass fractal dimension (1-3)

Greek letters

ν	kinematic viscosity, $m^2 \cdot s^{-1}$
β	particle collision kernel
λ	mean free path of the gas, m
σ_g	geometric mean deviation of size distribution

Abbreviation

B-QMOM	Bimodal QMOM
B-QMOMs	B-QMOM3 and B-QMOM4
B-log MM	Bimodal log-normal method of moments
B-TEMOM	Bimodal TEMOM
Log MM	Log-normal method of moments
MAD	Modal Aerosol Dynamics model
QMOM	Quadrature method of moments
TEMOM	Taylor expansion method of moments
SM	Sectional method

1. Introduction

Removal of micron or submicron particles through injection of relatively larger particles has been a promising technique for controlling fine particle emissions, especially for heavy metal emissions from combustion sources (Lee & Wu, 2005) and raindrop scavenging of aerosols (Jung et al., 2003; Lin & Gan, 2012; Yuan & Gan, 2013). A similar dynamic process also occurs in particle synthesis engineering (Buesser & Pratsinis, 2012), workplace aerosol emission (Anand et al., 2012), and dust storm and marine particles in the air (Whitby & McMurry, 1997; Jonasz, 2010). Brownian coagulation among different sized particles plays a key role in determining the evolution of size distribution in these particulate systems (Friedlander, 2000), whose dynamic process is theoretically governed by a population balance equation (PBE). However, such processes cannot be represented by a normal unimodal size distribution model (Whitby & McMurry, 1997; Lee & Wu, 2005). Today, there are several bimodal or multimodal mathematical models available to describe the above aerosol processes within the moment method framework (Whitby & McMurry, 1997; Ackermann et al., 1998; Jung et al., 2002; Jeong & Choi, 2004 & 2005; Lee & Wu, 2005). However, in all of these models, the fine particle mode is usually assumed to be monodisperse or all modes are assumed to be log-normal distributions, which may weaken the application of these models in real practice. Thus a much more reliable and computationally efficient bimodal model is proposed that does not require any assumption of size distribution (Yu & Seipenbusch, 2010).

For an aerosol with more than one mode, the size distribution function is generally described by multiple, independent component populations (Whitby & McMurry, 1997). The aerosol within each mode can then be approximated by a separated mode size distribution, usually a log-normal distribution. This methodology for investigating aerosol dynamics is usually called Modal Aerosol Dynamics (MAD) (Whitby & McMurry, 1997); in a MAD study, the entire size distribution for multiple modal aerosols is extensively represented by the following expression,

$$n(v) = \sum_{i=1}^{m} \frac{1}{3v} \frac{N_i}{\sqrt{2\pi}\ln\sigma_{g_i}} \exp\left[\frac{-\ln^2(v/v_{g_i})}{18\ln^2\sigma_{g_i}}\right] \quad (1)$$

where m is the number of modes; n is the particle number concentration intensity, which is a function of the particle volume, v; and N_i, v_{g_i} and σ_{g_i} are the total particle number concentration, the geometric mean volume and the geometric standard deviation of number distribution within each mode, respectively. In MAD studies, the multiple log-normal distributions shown in Eq. (1) must be implicitly included in the population balance equation to achieve the evolution of aerosol size distribution (Whitby & McMurry, 1997). This solution can be successfully performed primarily because of the existence of Lee's theory regarding the log-normal moment method (Lee & Chen, 1984). In the framework of the log-normal method of moments (Lee & Chen, 1984), the governing equation for each modal size distribution can be easily converted to moment equations for obtaining the three statistical quantities, namely the total particle number concentration, the geometric standard deviation of the number distribution, and the geometric mean volume. Therefore, the modal population balance equation can be largely simplified, which enables the MAD scheme to be a very computationally efficient and reliable method in aerosol studies (Whitby & McMurry, 1997; Jung et al., 2002). To the best of our knowledge, the MAD scheme along with Lee's log-normal method of moments (log MM) is currently the most practical method for characterizing the evolution of aerosol size and the chemical composite distribution, especially for modal studies on atmospheric aerosols involving transport (Ackermann et al., 1998).

Although Lee's log-normal method of moments has been successfully applied in the construction of MAD governing equations and also extensively used in aerosol studies (Ackermann

et al., 1998; Seinfeld & Pandis, 2012), the inherent shortcoming for artificially approximating each mode size distribution to be an individual log-normal distribution cannot be overcome (Pratsinis, 1988). In fact, since the first proposal of the method of moments in 1964 (Hulburt & Katz, 1964), there have been several methods of moments available for characterizing the evolution of aerosol size distribution from the viewpoint of statistics. Five prominent techniques, namely making a prior assumption for the shape of the aerosol size distribution (Lee et al., 1984; Pratsinis, 1988), approximating the integral moment by an n-point Gaussian quadrature (McGraw, 1997; Marchisio et al., 2003), assuming the pth-order polynomial form for the moments (Barrett & Jheeta, 1996), achieving closure using the interpolative method (Frenklach, 2002), and achieving closure using the Taylor-Expansion technique (Yu et al., 2008; Yu & Lin, 2009b), were proposed by different researchers. Due to the low computational costs in the last 10 years, these five methods of moments have been widely applied in aerosol research fields regarding specific requirements (Vogel et al., 2014). To the best of our knowledge, the method with n-point Gaussian quadrature (QMOM), as well as its variant versions such as the direct quadrature method of moments (DQMOM) (McGraw, 1997; Marchisio et al., 2003; Chan et al., 2010; Liu et al., 2011), is the most frequently used method of moments. The advantage of QMOM lies in its lack of requirement for the size distribution; thus, it is regarded as a more precise model than log MM (Yu & Lin, 2009a). Similar to the QMOM, the Taylor expansion method of moments (TEMOM) also has the advantage of not requiring an assumption of the aerosol size distribution; in particular, TEMOM has been verified as a highly reliable method by comparison with other methods of moments and the sectional method (Yu et al., 2008). Compared to QMOM, TEMOM exhibits a significant advantage in efficiency because it only requires solving three ordinary differential equations (ODEs) for the first three moments, whereas in the QMOM, six ODEs are required to obtain the same moments (Yu & Lin, 2009a, 2009b; Yu etal., 2011; Xie et al., 2012). Since the TEMOM has been firstly proposed in 2008 (Yu et al., 2008), it has been further developed for solving the population balance equation in terms of both numerical and analytical solutions (Yu & Lin, 2009b; Yu et al., 2015a, 2015b; Xie, 2015). But the further study for its capacity to resolve the bimodal or multimodal aerosol problems remains an unresolved issue (Yu & Seipenbusch, 2010; Liu & Gu, 2013).

In the present study, the TEMOM methodology is firstly introduced into the construction of the bimodal MAD models and it is further compared with the existing log MM and QMOM under the identical conditions. For convenience of distinguishing the models from each other, the three bimodal moment method models are called B-TEMOM, B-QMOM and B-log MM, respectively. The B-TEMOM governing equations are primarily derived using the Taylor expansion technique by which only three orders of Taylor expansion series are reserved. The aim of this work is to obtain the governing equations for B-TEMOM and further verify it by comparing it to B-QMOM and B-log MM. Since only submicron or larger agglomerates are concerned; thus, the coagulation kernel in the continuum-slip regime is used (Lee et al., 1997) and the Knudsen number used is up to 5. For the QMOM, 3-point and 4-point Gaussian quadratures are applied. The comparisons among these three bimodal moment method models are mainly performed when varying the difference of the total particle number concentration, the geometric standard deviation, the geometric mean volume and the mass fractal dimension between modes. The similarities and differences among these three moment methodologies are addressed. Although the sectional method (SM) is always expected as reference to validate the methods of moments, it is not introduced in the present study since the reliability of both B-log MM and B-QMOM models is sufficiently verified for this newly proposed and developed B-TEMOM model.

2. Theory

In the derivation, only two modes are considered correspondingly, the entire agglomerate size distribution is artificially divided into two systems, each representing one mode (Whitby & McMurry, 1997). In the establishment of bimodal models, the total volume concentration of the two separated distributions as an entity must be conserved, while the transfer of mass between modes varies with time (Yu & Seipenbusch, 2010). Based on the Smoluchowski mean-field theory, the equation for representing the evolution of particle number with size v with time for Mode 1 (Large Particle) is firstly provided (Yu & Seipenbusch, 2010),

$$\frac{\partial n(v,t)}{\partial t} = \underbrace{\frac{1}{2}\int_0^v \beta(v-v',v')n(v-v',t)n(v',t)dv' - n(v,t)\int_0^\infty \beta(v,v')n(v',t)dv'}_{\text{Within Mode 1}} + \underbrace{\int_0^v \beta(v-v',v')n(v-v',t)p(v',t)dv' - n(v,t)\int_0^\infty \beta(v,v')p(v',t)dv'}_{\text{Between Mode 1 and Mode 2}} \tag{2}$$

where $n(v,t)dv$ is the particle number of Mode 1, whose volume is between v and $v+dv$ at time t, and $\beta(v,v')$ is the collision kernel for two particles of volumes v and v'. On the right-hand side of Eq. (2), the first two terms account for the particle number increase and decrease due to intra-particle collisions and join together inside Mode 1, while the last two terms serve as the particle increase and loss due to inter-particle collisions between Mode 1 and Mode 2. $p(v',t)$ is the particle number with size v' for Mode 2. Similarly, the evolution of particle number with size v for Mode 2 (small particles) is then written in the following expression (Yu & Seipenbusch, 2010),

$$\frac{\partial p(v,t)}{\partial t} = \underbrace{\frac{1}{2}\int_0^v \beta(v-v',v')p(v-v',t)p(v',t)dv' - p(v,t)\int_0^\infty \beta(v,v')p(v',t)dv'}_{\text{Within Mode 2}} - \underbrace{p(v,t)\int_0^\infty \beta(v,v')n(v',t)dv'}_{\text{Between Mode 1 and Mode 2}} \tag{3}$$

On the right-hand side of Eq. (3), the first two terms account for the particle number increase and decrease due to intra-particle collisions and join together within Mode 2, while the last term serves as the particle loss due to inter-particle collision between Mode 1 and Mode 2.

In this study, the general procedure for the method of moments is followed in which it must convert the population balance equation with respect to the number concentration intensity into a set of ordinary differential equations with respect to moment (Hulburt & Katz, 1964). The moment transformation involves multiplying equations (2) and (3) by v^k and then integrating over the entire size distribution, and finally the transformed moment ordinary differential equations take the following expression,

$$\frac{dm_k}{dt} = \underbrace{\frac{1}{2}\int_0^\infty\int_0^\infty [(v_c+v_c')^k - v_c^{\,k} - v_c'^{\,k}]\beta(v_c,v_c')n(v_c,t)n(v_c',t)dv_c dv_c'}_{\text{Within Mode 1}} + \underbrace{\int_0^\infty\int_0^\infty [(v_c+v_c')^k - v_c^{\,k}]\beta(v_c,v_c')n(v_c,t)p(v_c',t)dv_c dv_c'}_{\text{Between Mode 1 and Mode 2}} \tag{4.1}$$

$$\frac{dl_k}{dt} = \underbrace{\frac{1}{2}\int_0^\infty \int_0^\infty [(v_c + v_c')^k - v_c^k - v_c'^k]\beta(v_c, v_c')p(v_c, t)p(v_c', t)dv_c dv_c'}_{\text{Within Mode 2}}$$

$$\underbrace{- \int_0^\infty \int_0^\infty v_c'^k \beta(v_c, v_c')p(v_c', t)n(v_c, t)dv_c dv_c'}_{\text{Between Mode 1 and Mode 2}} \tag{4.2}$$

Here, the k-th moment is defined as

$$m_k = \int_0^\infty v^k n(v)dv. \tag{5.1}$$

$$l_k = \int_0^\infty v^k l(v)dv. \tag{5.2}$$

where $k = 0,1,2,3,\cdots$. If only the first three moments are considered, then Eqs. (4.1) and (4.2) are expressed as the following coupled differential-integral system,

$$\begin{cases} \frac{dm_0}{dt} = -\frac{1}{2}\int_0^\infty \int_0^\infty \beta(v_c, v_c')n(v_c, t)n(v_c', t)dv_c dv_c' \\ \frac{dm_1}{dt} = \int_0^\infty \int_0^\infty v_c'\beta(v_c, v_c')n(v_c, t)p(v_c', t)dv_c dv_c' \\ \frac{dm_2}{dt} = \frac{1}{2}\int_0^\infty \int_0^\infty 2v_c v_c'\beta(v_c, v_c')n(v_c, t)n(v_c', t)dv_c dv_c' + \int_0^\infty \int_0^\infty [v_c'^2 + 2v_c v_c']\beta(v_c, v_c')n(v_c, t)p(v_c', t)dv_c dv_c' \\ \frac{dl_0}{dt} = -\frac{1}{2}\int_0^\infty \int_0^\infty \beta(v_c, v_c')p(v_c, t)p(v_c', t)dv_c dv_c' - \int_0^\infty \int_0^\infty \beta(v_c, v_c')p(v_c', t)n(v_c, t)dv_c dv_c' \\ \frac{dl_1}{dt} = -\int_0^\infty \int_0^\infty v_c'\beta(v_c, v_c')p(v_c', t)n(v_c, t)dv_c dv_c' \\ \frac{dl_2}{dt} = \frac{1}{2}\int_0^\infty \int_0^\infty 2v_c v_c'\beta(v_c, v_c')p(v_c, t)p(v_c', t)dv_c dv_c' - \int_0^\infty \int_0^\infty v_c'^2\beta(v_c, v_c')p(v_c', t)n(v_c, t)dv_c dv_c' \end{cases} \tag{6}$$

In the continuum plus near-continuum regime (Yu & Lin, 2009b), the coagulation rate for agglomerates, $\beta(v_c, v_c')$ is

$$\beta(v_c, v_c') = B_2\{\left(\frac{1}{v^f} + \frac{1}{v'^f}\right)\left(v^f + v'^f\right) + \emptyset v_{p0}^{f-\frac{1}{3}}\left(\frac{1}{v^{2f}} + \frac{1}{v'^{2f}}\right)(v^f + v'^f)\} \tag{7}$$

where v_c is the collision volume of agglomerates with $v_c = v_{p0}^{1-3/D_f} v^{3/D_f}$, $\emptyset = \lambda A/(3/4\pi)^{1/3}$, A = 1.591, $f = 1/D_f$, and v is the real volume of the agglomerate. Here, v_{p0} is the volume of primary particles whose diameter is specified to be 1 nm in the work, and D_f is the fractal dimension whose value is theoretically from 1 to 3. $B_2 = 2k_B T/3\mu$, where k_B is the Boltzmann constant, T denotes the air temperature, and μ denotes the gas viscosity. As Eq. (7) is introduced into Eq. (6), one can obtain the following expression,

$$
\begin{cases}
\dfrac{dm_0}{d(B_2t)} = -\dfrac{1}{2}\displaystyle\int_0^\infty\int_0^\infty \left[\xi_1 + \emptyset {v_{p0}}^{f-\frac{1}{3}}\xi_2\right] n(v,t)n(v',t)dvdv' \\
\dfrac{dm_1}{d(B_2t)} = \displaystyle\int_0^\infty\int_0^\infty \left[\eta_1 + \emptyset {v_{p0}}^{f-\frac{1}{3}}\eta_2\right] n(v,t)p(v',t)dvdv' \\
\dfrac{dm_2}{d(B_2t)} = \dfrac{1}{2}\displaystyle\int_0^\infty\int_0^\infty \left[\zeta_1 + \emptyset {v_{p0}}^{f-\frac{1}{3}}\zeta_2\right] n(v,t)n(v',t)dvdv' \\
\qquad\qquad + \displaystyle\int_0^\infty\int_0^\infty \left[(\varsigma_1 + \zeta_1) + (\varsigma_2 + \zeta_2)\emptyset {v_{p0}}^{f-\frac{1}{3}}\right] \beta(v,v')n(v,t)p(v',t)dvdv' \\
\dfrac{dl_0}{d(B_2t)} = -\dfrac{1}{2}\displaystyle\int_0^\infty\int_0^\infty \left[\xi_1 + \emptyset {v_{p0}}^{f-\frac{1}{3}}\xi_2\right] p(v,t)p(v',t)dvdv' - \displaystyle\int_0^\infty\int_0^\infty \left[\xi_1 + \emptyset {v_{p0}}^{f-\frac{1}{3}}\xi_2\right] p(v',t)n(v,t)dvdv' \\
\dfrac{dl_1}{d(B_2t)} = -\displaystyle\int_0^\infty\int_0^\infty \left[\eta_1 + \emptyset {v_{p0}}^{f-\frac{1}{3}}\eta_2\right] p(v',t)n(v,t)dvdv' \\
\dfrac{dl_2}{d(B_2t)} = \dfrac{1}{2}\displaystyle\int_0^\infty\int_0^\infty \left[\zeta_1 + \emptyset {v_{p0}}^{f-\frac{1}{3}}\zeta_2\right] p(v,t)p(v',t)dvdv' - \displaystyle\int_0^\infty\int_0^\infty \left[\varsigma_1 + \varsigma_2\emptyset {v_{p0}}^{f-\frac{1}{3}}\right] p(v',t)n(v,t)dvdv'
\end{cases}
\tag{8}
$$

with

$$\xi_1 = 2 + v^f v'^{-f} + v'^f v^{-f}$$
$$\xi_2 = v^{-f} + v^f v'^{-2f} + v'^f v^{-2f} + v'^{-f}$$
$$\eta_1 = 2v' + v^f v'^{-f+1} + v'^{f+1} v^{-f}$$
$$\eta_2 = v^{-f}v' + v^f v'^{-2f+1} + v'^{f+1} v^{-2f} + v'^{-f+1}$$
$$\zeta_1 = 4vv' + 2v^{1+f}v'^{1-f} + 2v^{1-f}v'^{1+f}$$
$$\zeta_2 = 2v^{1-f}v' + 2v^{1+f}v'^{1-2f} + 2v^{1-2f}v'^{1+f} + 2vv'^{1-f}$$
$$\varsigma_1 = 2v'^2 + v^f v'^{2-f} + v'^{f+2} v^{-f}$$
$$\varsigma_2 = v^{-f}v'^2 + v^f v'^{2-2f} + v'^{f+2} v^{-2f} + v'^{2-f}$$
$$\vartheta_1 = \varsigma_1 + \zeta_1$$
$$\vartheta_2 = \varsigma_2 + \zeta_2$$

Using the transformed Eqs. (5), the right-hand side terms of Eq. (8) can be integrated, using the same procedure presented in the unimodal TEMOM model (Yu et al., 2008; Yu & Lin, 2009a, 2009b). In this case, their detailed expressions take the following form:

$$
\begin{cases}
\dfrac{dm_0}{d(B_2t)} = -\dfrac{1}{2}\left[{\xi_1}^* + \emptyset {v_{p0}}^{f-\frac{1}{3}}{\xi_2}^*\right] \\
\dfrac{dm_1}{d(B_2t)} = \left[{\eta_1}^{**} + \emptyset {v_{p0}}^{f-\frac{1}{3}}{\eta_2}^{**}\right] \\
\dfrac{dm_2}{d(B_2t)} = \dfrac{1}{2}\left[{\zeta_1}^* + \emptyset {v_{p0}}^{f-\frac{1}{3}}{\zeta_2}^*\right] + \left[{\vartheta_1}^{**} + {\vartheta_2}^{**}\emptyset {v_{p0}}^{f-\frac{1}{3}}\right] \\
\dfrac{dl_0}{d(B_2t)} = -\dfrac{1}{2}\left[{\xi_1}^{*'} + \emptyset {v_{p0}}^{f-\frac{1}{3}}{\xi_2}^{*'}\right] - \left[{\xi_1}^{**} + \emptyset {v_{p0}}^{f-\frac{1}{3}}{\xi_2}^{**}\right] \\
\dfrac{dl_1}{d(B_2t)} = -\left[{\eta_1}^{**} + \emptyset {v_{p0}}^{f-\frac{1}{3}}{\eta_2}^{**}\right] \\
\dfrac{dl_2}{d(B_2t)} = \dfrac{1}{2}\left[{\zeta_1}^{*'} + \emptyset {v_{p0}}^{f-\frac{1}{3}}{\zeta_2}^{*'}\right] - \left[{\varsigma_1}^{**} + {\varsigma_2}^{**}\emptyset {v_{p0}}^{f-\frac{1}{3}}\right]
\end{cases}
\tag{9}
$$

where

$\xi_1^{*} = 2m_0m_0 + m_fm_{-f} + m_{-f}m_f$

$\xi_2^{*} = m_0m_{-f} + m_fm_{-2f} + m_fm_{-2f} + m_0m_{-f}$

$\xi_1^{*\prime} = 2l_0l_0 + l_fl_{-f} + l_{-f}l_f$

$\xi_2^{*\prime} = l_0l_{-f} + l_fl_{-2f} + l_fl_{-2f} + l_0l_{-f}$

$\xi_1^{**} = 2m_0l_0 + m_fl_{-f} + m_{-f}l_f$

$\xi_2^{**} = m_0l_{-f} + m_fl_{-2f} + l_fm_{-2f} + l_0m_{-f}$

$\eta_1^{**} = 2m_0l_1 + m_fl_{-f+1} + m_{-f}l_{f+1}$

$\eta_2^{**} = m_{-f}l_1 + m_fl_{-2f+1} + m_{-2f}l_{f+1} + m_0l_{-f+1}$

$\zeta_1^{*} = 4m_1m_1 + 2m_{1+f}m_{1-f} + 2m_{1+f}m_{1-f}$

$\zeta_2^{*} = 2m_{1-f}m_1 + 2m_{1+f}m_{1-2f} + 2m_{1-2f}m_{1+f} + 2m_1m_{1-f}$

$\zeta_1^{*\prime} = 4l_1l_{1-f} + 2l_{1+f}l_{1-f} + 2l_{1+f}l_{1-f}$

$\zeta_2^{*\prime} = 2l_{1-f}l_1 + 2l_{1+f}l_{1-2f} + 2l_{1-2f}l_{1+f} + 2l_1l_{1-f}$

$\varsigma_1^{**} = 2m_0l_2 + m_fl_{2-f} + m_{-f}l_{f+2}$

$\varsigma_2^{**} = m_{-f}l_2 + m_fl_{2-2f} + m_{-2f}l_{2+f} + m_0l_{2-f}$

$\zeta_1^{**} = 4m_1l_{1+f} + 2m_{1+f}l_{1-f} + 2m_{1-f}l_{1+f}$

$\zeta_2^{**} = 2m_{1-f}l_1 + 2m_{1-2f}l_{1+f} + 2m_{1+f}l_{1-2f} + 2m_1l_{1-f}$

$\vartheta_1^{**} = \varsigma_1^{**} + \zeta_1^{**}$

$\vartheta_2^{**} = \varsigma_2^{**} + \zeta_2^{**}$

In Eq. (9), most of the moment variables are of fractal-order, not integral moments. To further close the moment equation, these fractional moments must be converted to integer variables. Therefore, the TEMOM methodology is introduced here. The relevant closure equations are given by the following expression (Yu et al., 2008),

$$m_k = \left(\frac{u_m{}^{k-2}k^2}{2} - \frac{u_m{}^{k-2}k}{2}\right)m_2 + \left(-u_m{}^{k-1}k^2 + 2u_m{}^{k-1}k\right)m_1 + \left(u_m{}^{k} + \frac{u_m{}^{k}k^2}{2} - \frac{3u_m{}^{k}k}{2}\right)m_0 \tag{10}$$

$$l_k = \left(\frac{u_l{}^{k-2}k^2}{2} - \frac{u_l{}^{k-2}k}{2}\right)l_2 + \left(-u_l{}^{k-1}k^2 + 2u_l{}^{k-1}k\right)l_1 + \left(u_l{}^{k} + \frac{u_l{}^{k}k^2}{2} - \frac{3u_l{}^{k}k}{2}\right)l_0 \tag{11}$$

whereu_m and u_l u_m and u_l represent the Taylor-expansion point of Mode 1 and Mode 2, respectively. The criterion for choosing these points was provided in the previous established work (Yu et al., 2008). Hence, the Taylor-expansion point is taken as $u_m = \frac{m_1}{m_0}$ and $u_l = \frac{l_1}{l_0}$ in the present study. It is worth noting that actually the averaged particle volume at each particle size distribution is used for each Taylor expansion point. The reliability and accuracy of this newly proposed bimodal model (B-TEMOM) will be validated below through comparing it to the well-known and classical methods including QMOM and log MM.

In the present study, the log MM approach was proposed by Lee & Chen (1984) and Lee et al. (1997), which is then introduced and performed for tracing the evolution of bimodal size distributions for comparison, i.e., B-log MM. In the B-log MM model, the fractal moments are defined as a function of three quantities, namely m_0, v_{gm} and σ_{gm}, or l_0, v_{gl} and σ_{gl}, depending on which mode the particles belong to,

$$m_k = m_0v_{gm}{}^{k}\exp\left(\frac{9}{2}k^2\ln^2\sigma_{gm}\right) \tag{12}$$

$$l_k = l_0v_{gl}{}^{k}\exp\left(\frac{9}{2}k^2\ln^2\sigma_{gl}\right) \tag{13}$$

with $v_{gm} = \frac{{m_1}^2}{{m_0}^{3/2}{m_2}^{1/2}}$ and $\ln^2\sigma_{gm} = \frac{1}{9}\ln\left(\frac{m_0 m_2}{{m_1}^2}\right)$, or $v_{gl} = \frac{{l_1}^2}{{l_0}^{3/2}{l_2}^{1/2}}$ and $\ln^2\sigma_{gl} = \frac{1}{9}\ln\left(\frac{l_0 l_2}{{l_1}^2}\right)$. Here, v_g is the geometric mean volume and σ_g is the geometric standard deviation of the number distribution. Similar to the B-log MM and QMOM models (McGraw, 1997) are also introduced and used for constructing the bimodal moment method model for comparison. In the framework of QMOM, the fractal moments are represented by,

$$\begin{cases} m_k = \sum_{i=1}^{NQ} {q_i}^k \omega_i \\ l_k = \sum_{i=1}^{NQ} {y_i}^k \psi_i \end{cases} \tag{14}$$

where NQ is the order of the quadrature formulation, q_i and y_i are the ith quadrature points representing the particle volume in physics, and ω_i and ψ_i are the corresponding weights in the quadrature formula representing the number intensity. As equation (14) is used in Eqs. (4), the ordinary differential equations with respect to moment rather than the particle number concentration intensity take the following expression,

$$\frac{dm_k(t)}{dt} = \frac{1}{2}\sum_{i=1}^{NQ}\sum_{j=1}^{NQ}\left[\left(q_i + q_j\right)^k - {q_i}^k - {q_j}^k\right]\beta\left(q_i, q_j\right)\omega_i\omega_j + \sum_{i=1}^{NQ}\sum_{j=1}^{NQ}\left[\left(q_i + y_j\right)^k - {q_i}^k\right]\beta\ \left(q_i, y_j\right)\omega_i\psi_j$$

$$(k = 0,1,2,3,\cdots) \tag{15}$$

$$\frac{dl_k(t)}{dt} = \frac{1}{2}\sum_{i=1}^{NQ}\sum_{i=1}^{NQ}\left[\left(y_i + y_j\right)^k - {y_i}^k - {y_j}^k\right]\beta\left(y_i, y_j\right)\psi_i\psi_j - \sum_{i=1}^{NQ}\sum_{j=1}^{NQ}{y_i}^k\beta\ \left(q_i, y_j\right)\omega_i\psi_j$$

$$(k = 0,1,2,3,\cdots) \tag{16}$$

It should be noted that in the B-QMOM, three and four nodes of the quadrature are used, which means that there are a total of 12 and 16 coupled ordinary differential equations in B-QMOM3 and B-QMOM4, respectively, whereas in the B-TEMOM and B-log MM models, there are only 6 ordinary differential equations for each. The difference among B-QMOM, B-TEMOM and B-log MM models lies in the mathematical way for solving the governing equations as shown in Equations (2) and (3). Since the B-log MM has been widely acknowledged as a reliable method to study the bimodal aerosol dynamics, thus the B-TEMOM as shown in Equation (9), and B-QMOM as shown in Equations (15) and (16) are also reliable and accurate.

3. Simulation condition

The fourth-order Runge-Kutta method with a fixed time step of 0.001 is used to solve the B-TEMOM, B-QMOMs and B-log MM models. For all studied models, the total time steps are up to 1,000,000. Because the model is proposed for agglomerates whose primary particle size must be specified in the coagulation kernel shown in equation (7), the size of the primary particle is specified to be 1.0 nm in diameter in the present study. In the calculation, the dimensionless operation is used,

$$\begin{cases} m_k = {M_k}^* m_0 {v_{gm}}^k {\chi_m}^{k*k} \\ l_k = {L_k}^* l_0 {v_{gl}}^k {\chi_l}^{k*k} \end{cases} \tag{17}$$

Under these conditions, the initial values for ${M_k}^*$ and ${L_k}^*$ should be as follows

$$\begin{cases} {M_k}^*(0) = 1 \\ {L_k}^*(0) = 1 \end{cases} \tag{18}$$

Here, χ_m and χ_l are input physical quantities that must be specified. $\chi = e^{w_g^2/2}$, $w_g = 3\ln\sigma_{g0}$ and σ_{g0} are the initial geometric standard deviation for each mode. The Knudsen number of particles is strongly related to the mean free path of molecular gas; thus, the air temperature is required to be specified at 300 K in the present calculations. In this case, the mean free path of gas molecules is 68.413 nm. The mass fractal dimension for both modes, which is used to characterize the agglomerate morphology, is always the same in the calculation. It should be noted that in the results, all of the moments and times are presented in non-dimensional units, which are convenient for analysis and comparisons.

4. Results

In the continuum-slip regime, the coagulation kernel shown in Eq. (7) is only valid up to the Knudsen number of 5.0 (Lee et al., 1997). In this case, the bimodal moment method models proposed in the present study can be used for agglomerates whose collision geometric mean diameter is larger than ~ 27 nm, based on the definition,

$$\mathrm{Kn} = \frac{2\lambda}{d_g} \tag{19}$$

where Kn is the Knudsen number with respect to the particle geometric mean size, λ is the mean free path of gas molecules, and d_g is the collision geometric mean diameter of the agglomerates. This model meets the design criteria of the current research work for micron or larger agglomerates. With the limitation for the agglomerate geometric mean diameter in the present study, nine different initial bimodal size distributions are presented in Table 1. They are specifically designed to study the similarities and differences among B-TEMOM, B-QMOMs and B-log MM. In Table 1, the differences in the particle number concentration, geometric mean volume, geometric standard deviation of the number distribution between modes, and the fractal dimension are taken into consideration. Because the first three moments are usually considered as the key quantities in the method of moments (Lee et al., 1997; McGraw, 1997; Yu et al., 2008), they are selected as the main objective of the present study to enable a full comparison.

Table 1 Parameters of initial size distributions composed by two separated modes, each mode is characterized by four quantities, namely total particle number concentration (m_0 or l_0), geometric mean diameter (d_{gm} or d_{gl}), geometric standard deviation (σ_{gm} or σ_{gl}) and mass fractal dimension (D_{fm} or D_{fl}).

	Mode 1				**Mode 2**			
Distributions	m_{00}(#/m^3)	d_{gm0}(nm)	σ_{gm0}	D_{fm0}	l_{00}(#/m^3)	d_{gl0}(nm)	σ_{gl0}	D_{fl0}
1	7×10^{11}	200	1.40	3.00	1×10^{13}	50	1.40	3.00
2	7×10^{11}	1000	1.40	3.00	1×10^{13}	50	1.40	3.00
3	7×10^{11}	5000	1.40	3.00	1×10^{13}	50	1.40	3.00
4	7×10^{12}	1000	1.40	3.00	1×10^{13}	50	1.40	3.00
5	7×10^{10}	1000	1.40	3.00	1×10^{13}	50	1.40	3.00
6	7×10^{11}	200	1.40	2.50	1×10^{13}	50	1.40	2.50
7	7×10^{11}	200	1.40	2.00	1×10^{13}	50	1.40	2.00
8	7×10^{11}	1000	1.20	3.00	1×10^{13}	50	1.20	3.00
9	7×10^{11}	1000	1.01	3.00	1×10^{13}	50	1.01	3.00

4.1 Verification of the Studied Bimodal Moment Method Model Schemes

In theory, the total particle volume is conserved for any type of aerosols whose dynamic process is only dominated by the coagulation mechanism (Friedlander, 2000). Although the entire size distribution is artificially divided into two sub-systems in the present study, the total particle volume for two systems as an entity should be theoretically constant. Therefore, it is feasible to use the theory to preliminarily verify the bimodal moment method models whose size distribution is characterized by two separated sets of ordinary differential equations. In fact, a similar approach for separating the population balance equation for the entire size distribution into two component population balance equations for each mode is implemented in previous MAD studies (Whitby & McMurry, 1997). Here, D1 is selected to be presented in Table 1 as an example to be modeled by these four studied models, namely B-TEMOM, B-log MM, B-QMOM3 and B-QMOM4. The evolution of total volume of the entire size distribution produced by the four bimodal models is shown in Fig. 1. Each model clearly provides the same total particle volume, whose value is conserved with time, indicating that the solution for separating the entire distribution into two component distributions (Eqs. (2) and (3)) is feasible. This result further proves that Eqs. (2) and (3) are the correct population balance equations for characterizing the evolution of bimodal aerosols.

Fig.1 Evolution of total particle volume of a bimodal size distribution (D1) with time produced by four studied bimodal moment method models. $M_1=m_1/(m_{10}+l_{10})$.

4.2 Geometric mean particle volume

Fig.2 Comparison of dimensionless total M_0 and M_2 among different studied bimodal moment method models. $M_0= m_0/(m_{00}+l_{00})$, $M_2= m_2/(m_{20}+l_{20})$.

Fig.3 Comparison of dimensionless zeroth moment of both Mode 1 and Mode 2 obtained from B-TEMOM, B-QMOM3, B-QMOM4 and B-log MM models. $M_0= m_0/m_{00}$ for Mode 1, and $M_0= m_0/l_{00}$ for Mode 2.

Fig.4 Comparison of dimensionless first moment of Mode 2 obtained from B-TEMOM, B-QMOM3, B-QMOM4 and B-log MM models. $M1= m_1/(m_{10}+l_{10})$.

Fig.5 Comparison of dimensionless second moment of both Mode 1 and Mode 2 obtained from B-TEMOM,B-QMOM3, B-QMOM4 and B-log MM models. $M_2= m_2/m_{20}$ for Mode 1, and $L_2 = l_0/l_{20}$ for Mode 2.

The zeroth and the second moments are generally used as key quantities to verify a new method of moments (Yu et al., 2008) because for any aerosol that is solely dominated by the Brownian coagulation mechanism, the evolution of size distribution can be approximated by a log-normal distribution (Lee et al., 1997). In this case, only the first three moments are sufficient to evaluate whether a new model is reliable or not, which is applicable for all of the methods of moments for unimodal size distributions, including log MM, QMOM and TEMOM. However,

the same treatment cannot be directly extended to bimodal size distributions because coagulation occurs not only within each mode but also between modes. Thus, the bimodal model must be able to capture not only the total quantities of the entire size distribution but also the quantities of each mode (Jung et al., 2002; Jeong & Choi, 2004; Lee & Wu, 2005). Therefore, the comparisons among these four studied B-TEMOM, B-QMOM3, B-QMOM4 and B-log MM models within each mode are taken into consideration in the present study.

In a bimodal size distribution, the scavenging effect of Mode 1 on Mode 2 accounts for the main interaction mechanism between modes (Seipenbusch et al., 2008; Anand et al., 2012); thus, the differences in the geometric mean size, the magnitude and the geometric standard deviation between modes should be primarily considered. Similar works were performed in Jeong & Choi (2004) and Lee & Wu (2005). However, both of these previous works are limited to log-normal model studies with the model of Lee et al. (Lee & Chen, 1984). In the present study, the evolution of bimodal size distributions is firstly investigated in which only the geometric mean volume difference between modes is varied, whereas the geometric standard deviation and magnitude of each mode are the same. Fig. 2 shows the variance of dimensionless M_0 and M_2 of the entire size distribution with time produced by the four bimodal moment method models, namely B-TEMOM, B-QMOM3, B-QMOM4 and B-log MM. The parameters of three initial size distributions corresponding to D1, D2 and D3 are shown in Table 1. For the total particle number concentration M_0, all these four studied bimodal modes are found to provide nearly the same results. In particular, the curves obtained from B-QMOM3 and B-QMOM4 are found to overlap. As the geometric mean diameter difference is relatively small (D1), B-TEMOM and B-log MM provide the same results, and the two curves shown in Fig. 2 cannot be distinguished from each other. With the increase in the geometric mean diameter difference between the modes (D2 and D3), the difference between B-TEMOM and B-log MM slightly increases, but this only occurs at a later stage of evolution. For the total dimensionless second moment M_2, this solution indicates that all these four studied bimodal moment method models produce the same results for all three investigated distributions.

It has been generally acknowledged that only the first three moments, as shown in Figs. 1 and 2, cannot represent the detailed feature of a bimodal size distribution model, even though each mode accurately follows a log-normal or normal distribution (Whitby et al., 2002). This result is mainly because the size distribution with two modes cannot be reconstructed from the first three statistical moments. To further investigate the similarities and differences among the four investigated bimodal moment method models, the best way is to compare them within each mode. Fig. 3 shows the evolution of the dimensionless M_0 with time in respect to the initial distributions, D1, D2 and D3 within each mode produced by B-TEMOM, B-log MM, B-QMOM3 and B-QMOM4. For M_0 within Mode 1, B-TEMOM and B-log MM are found to produce nearly identical results, while QMOM3 and QMOM4 produce the same results. With the increase in the geometric standard size difference between modes, M_0 decreases more slowly, and the differences among the investigated bimodal moment method models also decrease. For M_0 within Mode 2, B-QMOM3 and B-QMOM4 also generate the same results, while B-TEMOM and B-log MM only produce the same result for D1. As the geometric mean volume difference is relatively large, a difference between B-TEMOM and B-log MM appears; in particular, the difference increases with the increase in the geometric mean volume difference. These solutions indicate that with the increase in the mean size difference, the number concentration within Mode 2 decreases much more quickly, which is the same as the conclusion from a bimodal log-normal model conducted in Lee & Wu (2005).

Although it is conserved for the entire size distribution, as shown in Fig. 1, the first moment within each mode still varies with time, and the variance is especially strongly dependent on the geometric mean volume difference

(Jung et al., 2002). Unlike the zeroth moment, whose variance within each mode is involved in intra-coagulation and inter-coagulation, the first moment is only involved in the transfer of volume concentration between modes, suggesting that it is only affected by inter-coagulation. Thus, the first moment should be another important quantity to reflect the feature of a bimodal moment method model, which differs absolutely from the zeroth moment. However, a study on the feature of a bimodal moment method model using the first moment as an index has never been performed up to date. Fig. 4 shows that for the comparison of the first moments, M_1, within Mode 2, the initial distributions are selected to be D1, D2 and D3, respectively. It shows that there is a difference among B-QMOMs, B-TEMOM and B-log MM, especially with the increase in the geometric mean volume difference, where the difference increases, but B-QMOM3 and B-QMOM4 always provide the same result.

In addition to the zeroth and first moments, the second moment should also be used for studying the feature of a mathematical bimodal moment method model. In fact, the second moment is usually used as an important index to verify unimodal models involving Brownian coagulation (Yu et al., 2008). Fig. 5 shows the comparison among different bimodal moment method models for the dimensionless second moment within each mode. Within Mode 1, all these four studied bimodal moment method models produce the same results for all three investigated initial distributions, and all curves for each initial distribution cannot be distinguished from each other. Within Mode 2, there is a relatively small difference among them, especially at a later stage. Similar to M_0 and M_1 as shown in Figs. 3 and 4, the differences among B-TEMOM, B-QMOMs and B-log MM also decrease with the decrease in the geometric mean volume difference.

In conclusion, these solutions indicate that although B-TEMOM, B-QMOMs and B-log MM provide very similar results for the first three moments for both decomposed component distributions within each mode and the whole distribution, the similarities among them are verified to be significantly affected by the geometric mean volume difference between modes. With the decrease in the volume difference, the difference among them also decreases. However, the QMOMs (i.e., QMOM3 and B-QMOM4) with three and four points are always the same for all of the investigated quantities.

4.3 Particle number concentration

Fig.6 Comparison of dimensionless zeroth moment of both Mode 1 and Mode 2 obtained from B-TEMOM, B-QMOM3, B-QMOM4 and B-log MM models. $M_0 = m_0/m_{00}$ for Mode 1, and $M_0 = m_0/l_{00}$ for Mode 2.

Fig.7 Comparison of dimensionless first and second moments within Mode 2 obtained from B-TEMOM, B-QMOM3, B-QMOM4 and B-log MM models.

The particle number concentration difference between modes significantly influences the scavenging effect of Mode 1 on Mode 2, which was verified in Jung et al. (2002) and Lee & Wu (2005). As the particle number concentration differences increases, the particles within Mode 2 are much easier to be removed, which is attributed to the stronger inter-coagulation between modes. Here, these four studied bimodal moment method models are used to compare the performance of each model for capturing the evolution of the first three moments within each mode.

Fig. 6 shows the dimensionless M_0 within Mode 1 and Mode 2 with the initial distributions selected to be D2, D4 and D5 presented in Table 1. In these distributions, only the total particle number concentrations between modes are different. For Mode 1, B-TEMOM and B-log MM clearly provide the same dimensionless M_0, but they have slightly different values compared to those of the B-QMOMs. However, the difference between B-TEMOM (or B-log MM) and the B-QMOMs decreases with the decrease in the particle number concentration difference between the modes. This is the same as the geometric mean volume difference investigated in Section 4.2. Although the differences among B-TEMOM, B-log MM and B-QMOMs are more obvious in Mode 2 than in Mode 1, the differences among them are also decreased with the decrease in the particle number concentration difference between two modes. The same features are also shown in Fig. 7 for dimensionless M_1 and M_2 within Mode 2. The observation indicates that the studied bimodal moment method models pose a relatively larger difference for the first three moments as the particle number concentration difference is increased, even though this difference is very small, especially at an initial stage of evolution.

4.4 Particle mass fractal dimension

Fig.8 Comparison of dimensionless zeroth moment of both Mode 1 and Mode 2 obtained from B-TEMOM, B-QMOM3, B-QMOM4 and B-log MM models. $M_0= m_0/m_{00}$ for Mode 1, and $M_0= m_0/l_{00}$ for Mode 2.

Fig.9 Comparison of dimensionless first and second moments within Mode 2 obtained from B-TEMOM, B-QMOM3, B-QMOM4 and B-log MM models.

The dynamics of agglomerates differs significantly from that of spherical counterparts, whose structures can be determined by a variable in a statistical sense, i.e., the fractal dimension D_f. The effect of the fractal dimension on agglomerate growth and size distribution is studied by Vemury & Pratsinis (1995) and Kazakov & Frenklach (1998); Park & Lee (2002); Dekkers & Friedlander (2002), Yu & Lin (2009b). These works are usually limited to one-modal size distribution or homodisperse aerosol systems. Although a novel bimodal moment method model is proposed for fractal-like agglomerates, each mode must follow a monodisperse size distribution in view of particle volume from Jeong & Choi (2003) for achieving the highest efficiency. Under these conditions, the information of a bimodal size distribution, especially the coagulation process within each mode, might be largely lost. In the present study, the size distribution is artificially divided into two component systems, with each system being involved in both inter-coagulation and intra-coagulation. This use of two component systems ensures that the dynamic process of coagulation can be reasonably revealed in the model.

D_f is well-known to play a significant role in the evolution of agglomerates dominated by Brownian coagulation (Yu & Lin, 2009b). Thus, D_f may affect the variance of the statistical moment quantities with time at each mode, as well as the feature of each bimodal moment method model, to capture the evolution of the agglomerates. Fig. 8 shows the dimensionless M_0 within each mode in respect to time produced by these four studied bimodal moment method models, which indicates that with the increase in D_f, the particles at both modes decreases much more quickly. This behavior is in contrast to those in the free molecular regime and in the transient regime (Yu & Lin, 2009b). The reason for this behavior should be that the collision surface between two colliding particles increases with the increase in D_f, thus increasing the coagulation efficiency. The detailed comparison of

the coagulation efficiency among different Df values can be referred to Fig. 1 of Yu & Lin (2009b). In the continuum-slip regime, especially in the continuum regime, the coagulation efficiency increases with the increase in D_f. For the three investigated initial distributions, both B-TEMOM and B-log MM are found to act as nearly the same model for generating M_0, while B-QMOM3 and B-QMOM4 are actually the same and cannot be distinguished from each other.

The comparisons among these four studied bimodal moment method models are also performed for dimensionless M_1 and M_2. Because the variance of the statistical moments in Mode 2 is much more clear than that in Mode 1, only the dimensionless M_1 and M_2 in Mode 2 are provided in the present study. Fig. 9 shows the evolution of the dimensionless M_1 and M_2 in Mode 2 with time obtained from these four studied bimodal moment method models. It also shows that B-QMOM3 and B-QMOM4 models produce the same results for both quantities, while B-log MM and B-TEMOM exhibit an obvious difference for both quantities. The difference between B-log MM and B-TEMOM is found to increase with a decrease in D_f, especially at a later stage in the evolution.

4.5 Geometric standard deviation

Fig. 10 Comparison of geometric standard deviation with time produced by B-TEMOM, B-log MM and B-QMOM3 (D1) models.

Fig.11 Comparison of dimensionless zeroth moment of both Mode 1 and Mode 2 obtained from B-TEMOM, B-QMOM3 and B-log MM models. $M_0 = m_0/m_{00}$ for Mode 1 and $M_0 = m_0/l_{00}$ for Mode 2.

Fig.12 Comparison of dimensionless first and second moments within Mode 2 obtained from B-TEMOM, B-QMOM3 and B-log MM models.

In log-normal distribution theory, the geometric standard deviation accounting for the spectrum of a size distribution can be represented by the first three moments (S. Pratsinis, 1988),

$$\log^2\sigma_g = \frac{1}{9}\ln\left(\frac{m_0 m_2}{m_1{}^2}\right) \tag{20}$$

where σ_g is the geometric standard deviation of the number concentration. Although Equation (20) is derived from the log normal theory, it has been verified as a reliable equation in both TEMOM and QMOM methods for solving the Brownian dynamics (Yu & Lin, 2009b). In the present study of bimodal moment method models, the same quantity can also be used to characterize the spectrum of each mode in the size distributions (Lee & Wu, 2005). It is well known that the geometric standard deviation of a log-normal distributed unimodal aerosol approaches 1.32 in the continuum regime and 1.345 in the free molecular regime for spherical particles (Lee et al., 1997). Although the effect of the inter-coagulation mechanism on the geometric standard deviation is studied in Lee & Wu (2005) with the absence of intra-coagulation in fine particle mode, the study with the presence of intra-coagulation in each mode and inter-coagulation between modes has not been previously performed. Similar to

the work in Lee & Wu (2005) for the initial geometric standard deviation, the geometric standard deviation of Mode 2 is also selected to be 1.4 in the present study, as shown in Fig. 10. The initial distribution here corresponds to D1 presented in Table 1. Although the differences in the results obtained from the bimodal moment method models are obvious, all of the geometric standard deviations are observed to decrease with the evolution; the same conclusion was obtained in the work of Lee & Wu (2005). It should be noted that B-QMOM3 produces the geometric standard deviation whose trend slightly deviates from B-TEMOM and B-log MM at a later stage.

In this section, the first three moments at each mode obtained from the B-TEMOM, B-log MM and B-QMOM3 as a function of the initial geometric standard deviation are compared. This comparison is performed because the geometric standard deviation was found to also affect the evolution of the bimodal size distribution (Jeong & Choi, 2004; Lee & Wu, 2005), in a manner similar to the number concentration and volume differences between modes. The investigated initial distributions correspond to D2, D8 and D9 presented in Table 1. Fig. 11 shows the dimensionless M_0 at both Mode 1 and Mode 2 produced by B-TEMOM, B-log MM and B-QMOM3. Here, the results obtained from B-QMOM4 are not shown because it always has the same curves as B-QMOM3 for all of the investigated statistical moments. With an increase in the geometric standard deviation, the particle number concentration M_0 is found to decrease faster in Mode 1, while it increases in Mode 2. This result mainly occurs because Mode 2 has a much stronger scavenging effect on Mode 1 due to the large geometric standard deviation. This behavior is the same as the finding in Lee & Wu (2005). In addition, with a decrease in the geometric standard deviation, the differences among B-TEMOM, B-log MM and B-QMOM3 models obviously decrease; in particular, the curves of these three studied bimodal moment method models are nearly merged into one curve for D9. The same feature is also shown in Fig. 12 for the dimensionless M_1 and M_2 in Mode 2, indicating that these three studied bimodal moment method models are much closer to each other with the decrease in the geometric standard deviation; finally, they can become one model as the initial distribution becomes monodisperse.

5. Conclusions

A novel bimodal moment method model is developed for submicron or larger agglomerates whose dynamic process is solely dominated by Brownian coagulation via separation of the whole bimodal size distribution into two individual component distributions. In this model scheme, each distribution is represented by its individual governing equation. These governing equations are solved using the existing TEMOM morphology. In the specific performance of the methods of moments, three orders of Taylor expansion series are applied in the TEMOM, while the third and fourth quadrature points are applied in the QMOM.

In the present study, the similarities and differences among B-TEMOM, B-log MM, B-QMOM3 and B-QMOM4 for producing the first three moments within each mode are mainly investigated. The results are fully verified that B-QMOM3 and B-QMOM4 always produce the same statistical moment quantities, indicating that the third quadrature point is sufficient for constructing a bimodal moment method model with high precision. Compared to B-QMOMs, B-TEMOM and B-log MM are much closer for the first three moments. The differences among the studied bimodal moment method models for the first three moments within each mode are fully verified to decrease with the decrease in the particle number concentration, the geometric standard deviation, and the geometric mean particle volume differences between two modes. In addition, the differences between B-log MM and B-TEMOM are found to increase with the decrease in D_f, especially at a later stage in the evolution. The solution fully verifies by this newly developed B-TEMOM which is reliable for predicting agglomerate dynamics undergoing Brownian coagulation in the continuum-slip regime.

6. Acknowledgements

This work was supported by the grants from the General Research Fund, Research Grants Council of the Hong Kong Special Administrative Region, China (Project No. PolyU 5101/13E) and the Central Research Grant of The Hong Kong Polytechnic University (Project No. B-Q39E).

7. References

Ackermann, I. J., Hass, H., Memmesheimer, M., Ebel, A., Binkowski, F. S., & Shankar, U.M.A. (1998). Modal Aerosol Dynamics Mode for Europe: Development and first applications. *Atmospheric Environment*, 32(17), 2981–2999.

Anand, S., Mayya, Y. S., Yu, M.Z., Seipenbusch, M., & Kasper, G. (2012). A numerical study of coagulation of nanoparticle aerosols injected continuously into a large, well stirred chamber. *Journal of Aerosol Science*, 52, 18–32.

Barrett, J. C., & Jheeta, J. S. (1996). Improving the accuracy of the moments method for solving the aerosol general dynamic equation. *Journal of Aerosol Science*, 27(8), 1135–1142.

Buesser, B., & Pratsinis, S. E. (2012). Design of nanomaterial synthesis by aerosol processes. *Annual Review of Chemical and Biomolecular Engineering*, 3, 103–27.

Chan, T.L., Liu, Y.H., & Chan C.K. (2010) Direct quadrature method of moments for the exhaust particle formation and evolution in the wake of the studied ground vehicle. *Journal of Aerosol Science*, 41(6), 553-568.

Dekkers, P. J., & Friedlander, S. K. (2002). The self-preserving size distribution theory. I. Effects of the Knudsen number on aerosol agglomerate growth. *Journal of Colloid and Interface Science*, 248(2), 295–305.

Friedlander, S. K. (2000). *Smoke, Dust and Haze: Fundamentals of Aerosol Behavior*. (G.L. Rogers, Ed.), 2nd ed., John Wiley & Sons, Inc., New York Wiley Interscience.

Frenklach, M. (2002). Method of moments with interpolative closure. *Chemical Engineering Science*, 57(12), 2229–2239.

Hulburt, H. M., & Katz, S. (1964). Some problems in particle technology- A statistical mechanical formulation. *Chemical Engineering Science*, 19(8), 555–574.

Jeong, J., & Choi, M. (2003). A simple bimodal model for the evolution of non-spherical particles undergoing nucleation, coagulation and coalescence. *Journal of Aerosol Science*, 34(8), 965–976.

Jeong, J. I., & Choi, M. (2004). A bimodal moment model for the simulation of particle growth. *Journal of Aerosol Science*, 35(9), 1071–1090.

Jeong, J. I., & Choi, M. (2005). A bimodal particle dynamics model considering coagulation, coalescence and surface growth, and its application to the growth of titania aggregates. *Journal of Colloid and Interface Science*, 281(2), 351–9.

Jonasz, M. (2010). Approximation of the size distribution of marine particles by a sum of log-normal functions. *Limnology and Oceanography*, 41(4), 744–754.

Jung, C., Kim, Y., & Lee, K. (2002). Simulation of the influence of coarse mode particles on the properties of fine mode particles. *Journal of Aerosol Science*, 33, 1201–1216.

Jung, C. H., Kim, Y. P., & Lee, K. W. (2003). A moment model for simulating raindrop scavenging of aerosols. *Journal of Aerosol Science*, 34(9), 1217–1233.

Kazakov, A., & Frenklach, M. (1998). Dynamic modeling of soot particle coagulation and aggregation: implementation with the method of moments and application to high-pressure laminar premixed flames. *Combustion and Flame*, 114(3-4), 484–501.

Lee, K. W., Chen, H., & Gieseke, J. A. (1984). Log-Normally Preserving Size Distribution for Brownian Coagulation in the Free-Molecule Regime. *Aerosol Science and Technology*, 3(1), 53–62.

Lee, K. W., & Chen, H. (1984). Coagulation Rate of Polydisperse Particles. *Aerosol Science and Technology*, 3(3), 327–334.

Lee, K., Lee, Y., & Han, D. (1997). The log-normal size distribution theory for Brownian coagulation in the low Knudsen number regime. *Journal of Colloid and Interface Science*, 492(188), 486–492.

Lee, S.R., & Wu, C.Y. (2005). Size Distribution Evolution of Fine Aerosols Due to Intercoagulation with Coarse Aerosols. *Aerosol Science and Technology*, 39(4), 358–370.

Lin, J.-Z., & Gan, F.J. (2012). Simulation of the Brownian coagulation of nanoparticles with initial bimodal size distribution via moment method. *Acta Mechanica Sinica*, 28(5), 1227–1237.

Liu, Y.H., He, Z., & Chan, T.L. (2011) Three-dimensional simulation of exhaust particle dispersion and concentration fields in the near-wake region of the studied ground vehicle. *Aerosol Science and Technology* 45(8), 1019-1030.

Liu, Y.H., & Gu, H. (2013). The Taylor-expansion method of moments for the particle system with bimodal distribution. Thermal Science, 17(5), 1542–1545.

Marchisio, D. L., Vigil, R. D., & Fox, R. O. (2003). Quadrature method of moments for aggregation-breakage processes. *Journal of Colloid and Interface Science*, 258(2), 322–334.
McGraw, R. (1997). Description of Aerosol Dynamics by the Quadrature Method of Moments. *Aerosol Science and Technology*, 27(2), 255–265.
Park, S. H., & Lee, K. W. (2002). Change in particle size distribution of fractal agglomerates during Brownian coagulation in the free-molecule regime. *Journal of Colloid and Interface Science*, 246(1), 85–91.
Pratsinis, S. (1988). Simultaneous nucleation, condensation, and coagulation in aerosol reactors. *Journal of Colloid and Interface Science*, 124(2), 416–427.
Seinfeld, J. H., & Pandis, S. N. (2012). *Atmospheric chemistry and physics: from air pollution to climate change*. John Wiley & Sons.
Seipenbusch, M., Binder, a, & Kasper, G. (2008). Temporal evolution of nanoparticle aerosols in workplace exposure. *The Annals of Occupational Hygiene*, 52(8), 707–16.
Vemury, S., & Pratsinis, S. E. (1995). Self-preserving size distributions of agglomerates. *Journal of Aerosol Science*, 26(2), 175–185.
Vogel, U., Savolainen, K., Wu, Q., van Tongeren, M., Brouwer, D., & Berges, M. (2014). *Handbook of Nanosafety: Measurement, Exposure and Toxicology*. Elsevier.
Whitby, E. R., & McMurry, P. H. (1997). Modal Aerosol Dynamics Modeling. *Aerosol Science and Technology*, 27(6), 673–688.
Whitby, E., Stratmann, F., & Wilck, M. (2002). Merging and remapping modes in modal aerosol dynamics models : a "Dynamic Mode Manager." *Journal of Aerosol Science*, 33(4), 623–645.
Xie, M.L., Yu, M.Z., Wang, L.P. (2012) A TEMOM model to simulate nanoparticle growth in the temporal mixing layer due to brownian coagulation. *Journal of Aerosol Sci*ence 54, 32–48.
Xie, M.L. (2015). Asymptotic solution of moment approximation of the particle population balance equation for Brownian agglomeration. *Aerosol Science and Technology*, 46, 109-114.
Yu, M.Z., Lin, J.Z., & Chan, T.L. (2008). A New Moment Method for Solving the Coagulation Equation for Particles in Brownian Motion. *Aerosol Science and Technology*, 42(9), 705–713.
Yu, M.Z, & Lin, J.Z. (2009a). Solution of the agglomerate Brownian coagulation using Taylor-expansion moment method. *Journal of Colloid and Interface Science*, 336(1), 142–9.
Yu, M.Z., & Lin, J.Z. (2009b). Taylor-expansion moment method for agglomerate coagulation due to Brownian motion in the entire size regime. *Journal of Aerosol Science*, 40(6), 549–562.
Yu, M.Z., & Seipenbusch, M. (2010). A bimodal moment method for aerosol coagulation using TEMOM model. In *International Aerosol Conference 2010*. Helsinki, Finland.
Yu, M.Z., Lin, J.Z., Jin, H., & Jiang, Y. (2011). The verification of the Taylor-expansion moment method for the nanoparticle coagulation in the entire size regime due to Brownian motion. *Journal of Nanoparticle Research*, 13(5), 2007–2020.
Yu, M.Z., Zhang, X.T., Jin, G.D., Lin, J.Z., & Seipenbusch, M. (2015a) A new analytical solution for solving the population balance equation in the continuum-slip regime. *Journal of Aerosol Sci*ence, 80, 1-10.
Yu, M.Z., Lin, J.Z., Cao, J.J., & Seipenbusch, M. (2015b) An analytical solution for the population balance equation using a moment method. Particuology, 18, 194-200.
Yuan, F., & Gan, F. (2013). Evolution of Aerosol Particles in the Rainfall Process via Method of Moments. *Abstract and Applied Analysis*, *2013*, 1–7.

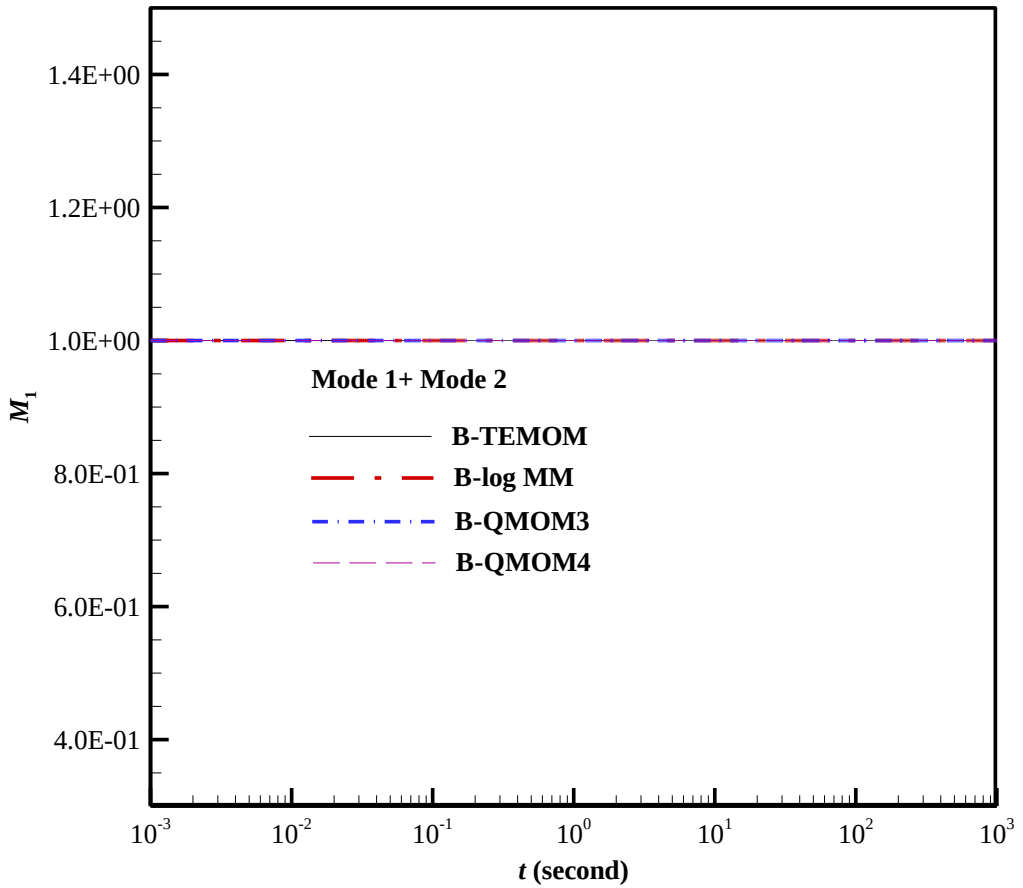

Fig.1 Evolution of total particle volume of a bimodal size distribution (D1) with time produced by four studied bimodal moment method models. $M_1 = \mathrm{m}_1/(m_{10} + l_{10})$.

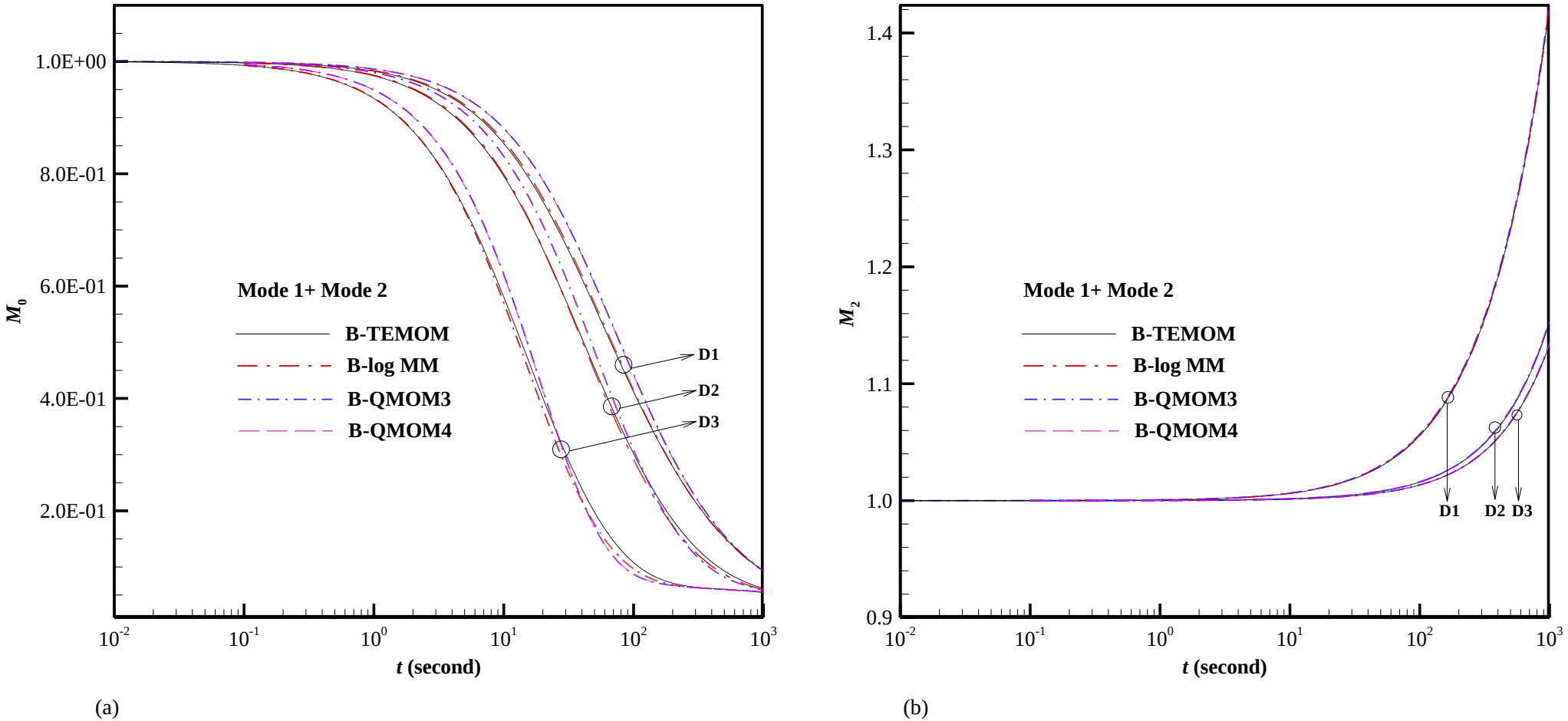

Fig.2 Comparison of dimensionless total M_0 and M_2 among different bimodal moment method models. $M_0 = m_0/(m_{00} + l_{00})$, $M_2 = m_2/(m_{20} + l_{20})$.

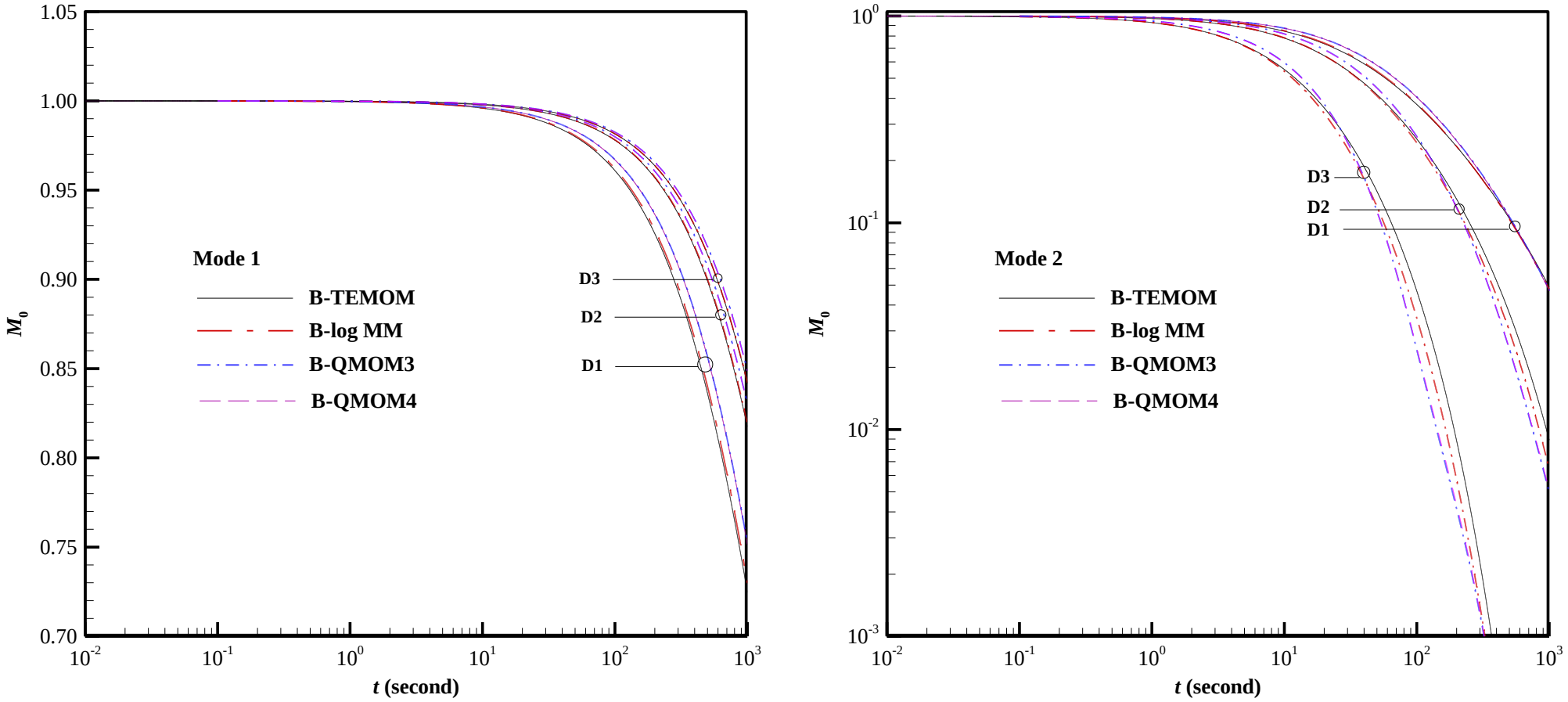

(a) (b)

Fig.3 Comparison of dimensionless zeroth moment of both Mode 1 and Mode 2 obtained from B-TEMOM, B-QMOM3, B-QMOM4 and B-log MM models. $M_0 = \mathrm{m}_0/m_{00}$ for Mode 1, and $M_0 = \mathrm{m}_0/l_{00}$ for Mode 2.

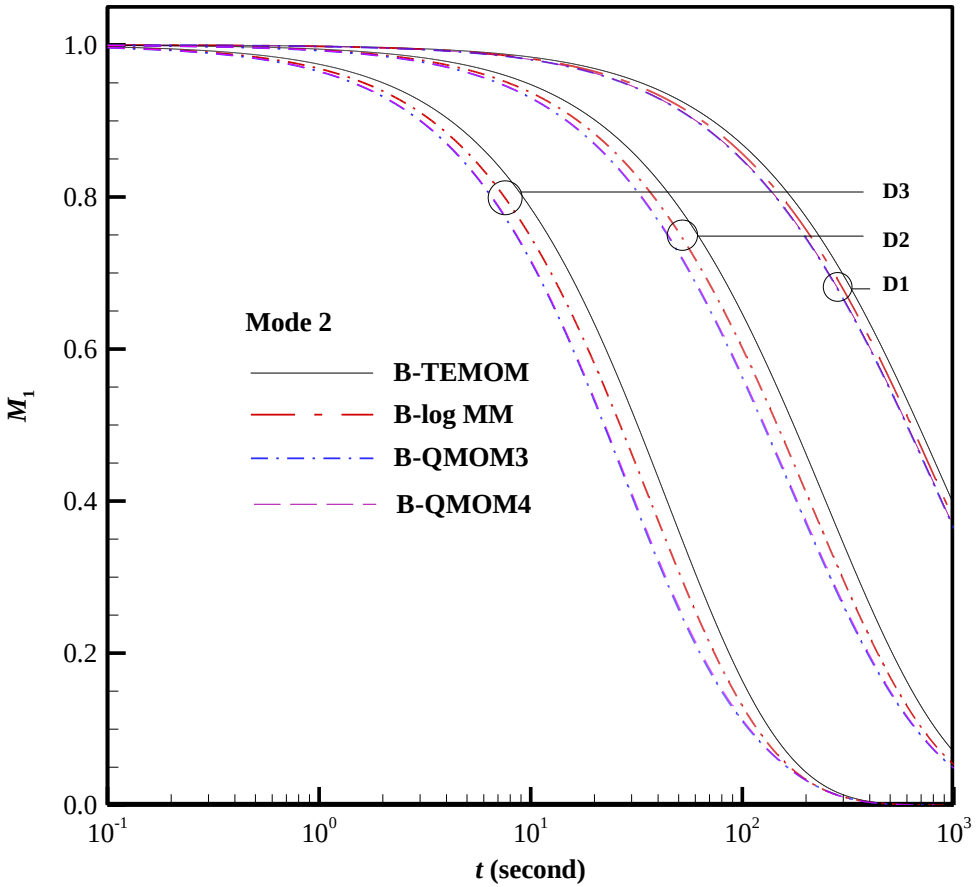

Fig.4 Comparison of dimensionless first moment of Mode 2 obtained from B-TEMOM, B-QMOM3, B-QMOM4 and B-log MM models. $M_1 = \mathrm{m}_1/(m_{10} + l_{10})$.

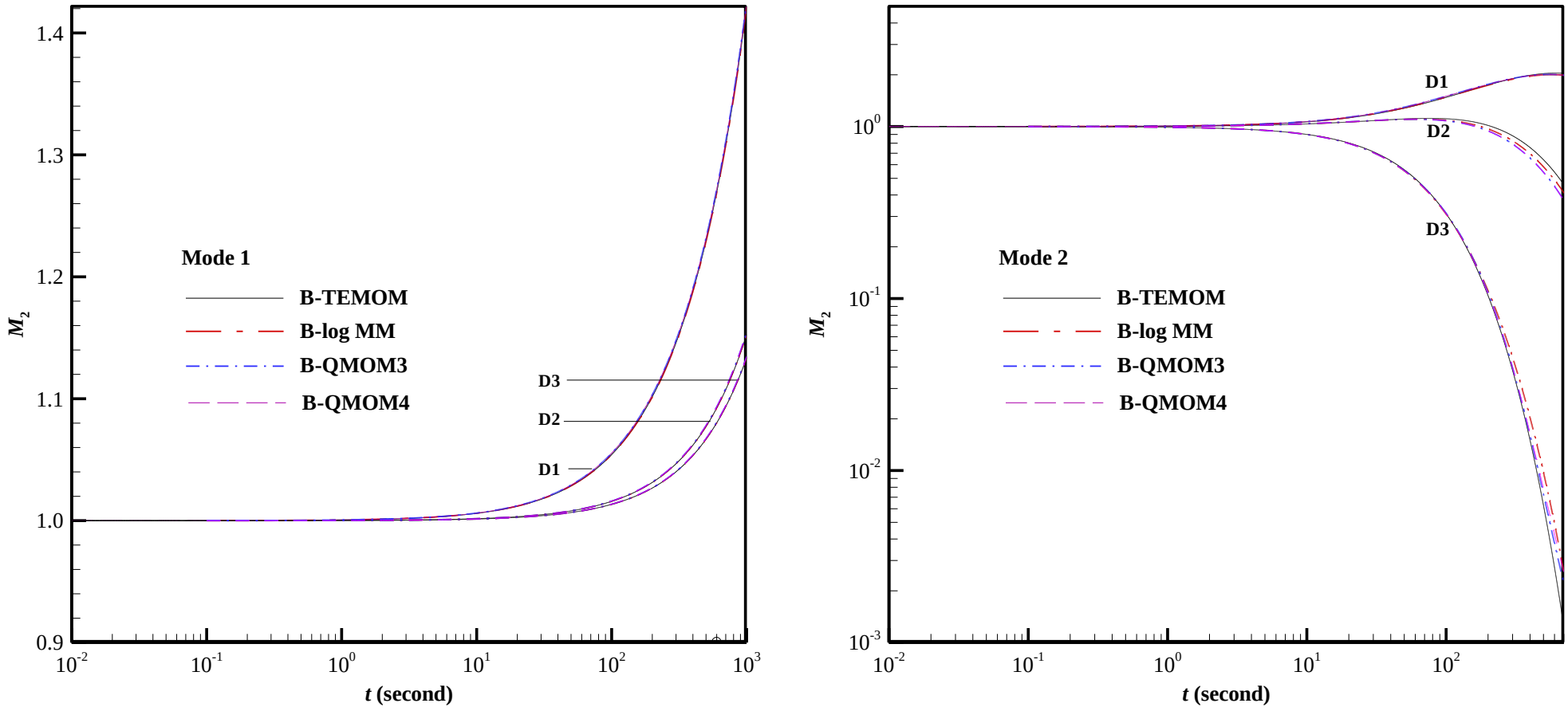

(a) (b)

Fig.5 Comparison of dimensionless second moment of both Mode 1 and Mode 2 obtained from B-TEMOM, B-QMOM3, B-QMOM4 and B-log MM models. $M_2 = m_2/m_{20}$ for Mode 1, and $M_2 = l_0/l_{20}$ for Mode 2.

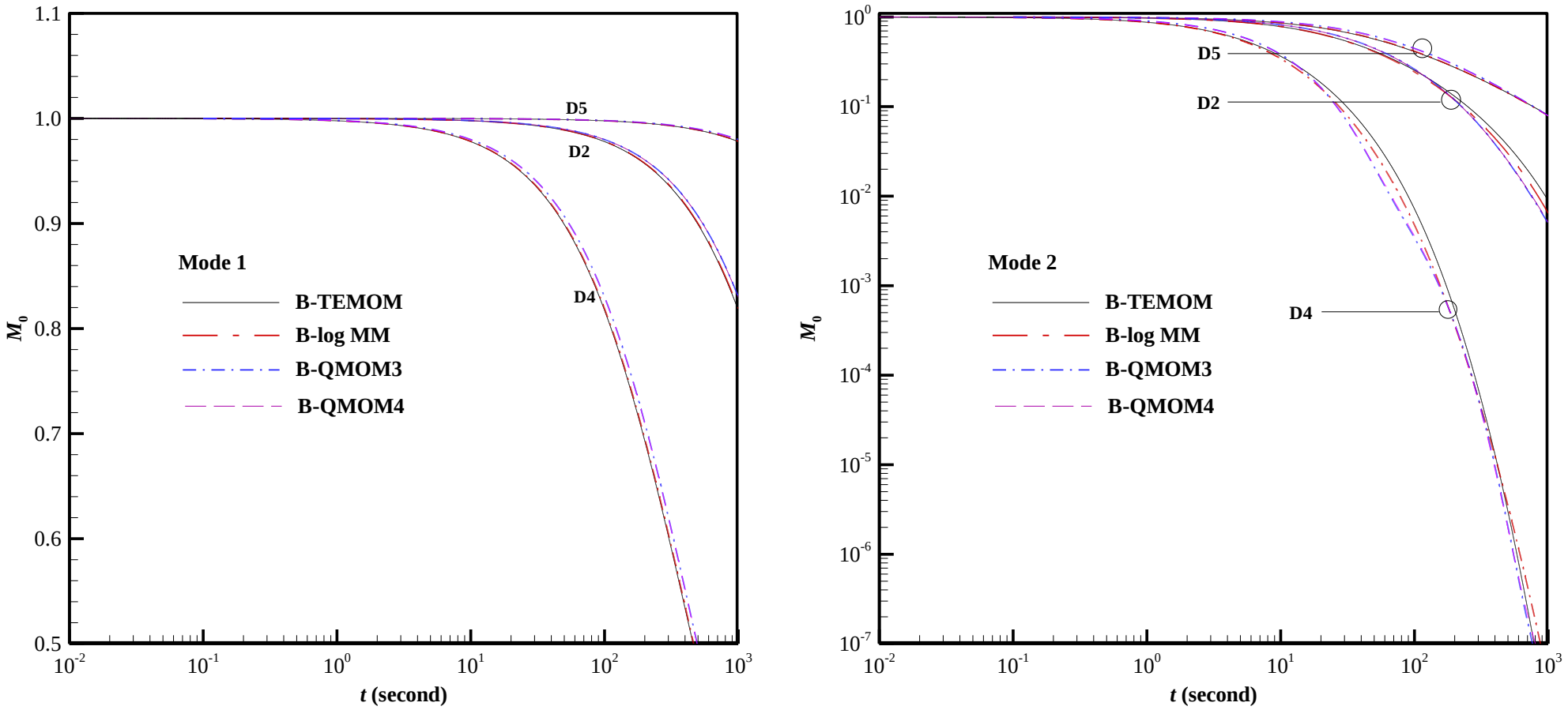

(a) (b)

Fig.6 Comparison of dimensionless zeroth moment of both Mode 1 and Mode 2 obtained from B-TEMOM, B-QMOM3, B-QMOM4 and B-log MM models. $M_0 = m_0/m_{00}$ for Mode 1, and $M_0 = m_0/l_{00}$ for Mode 2.

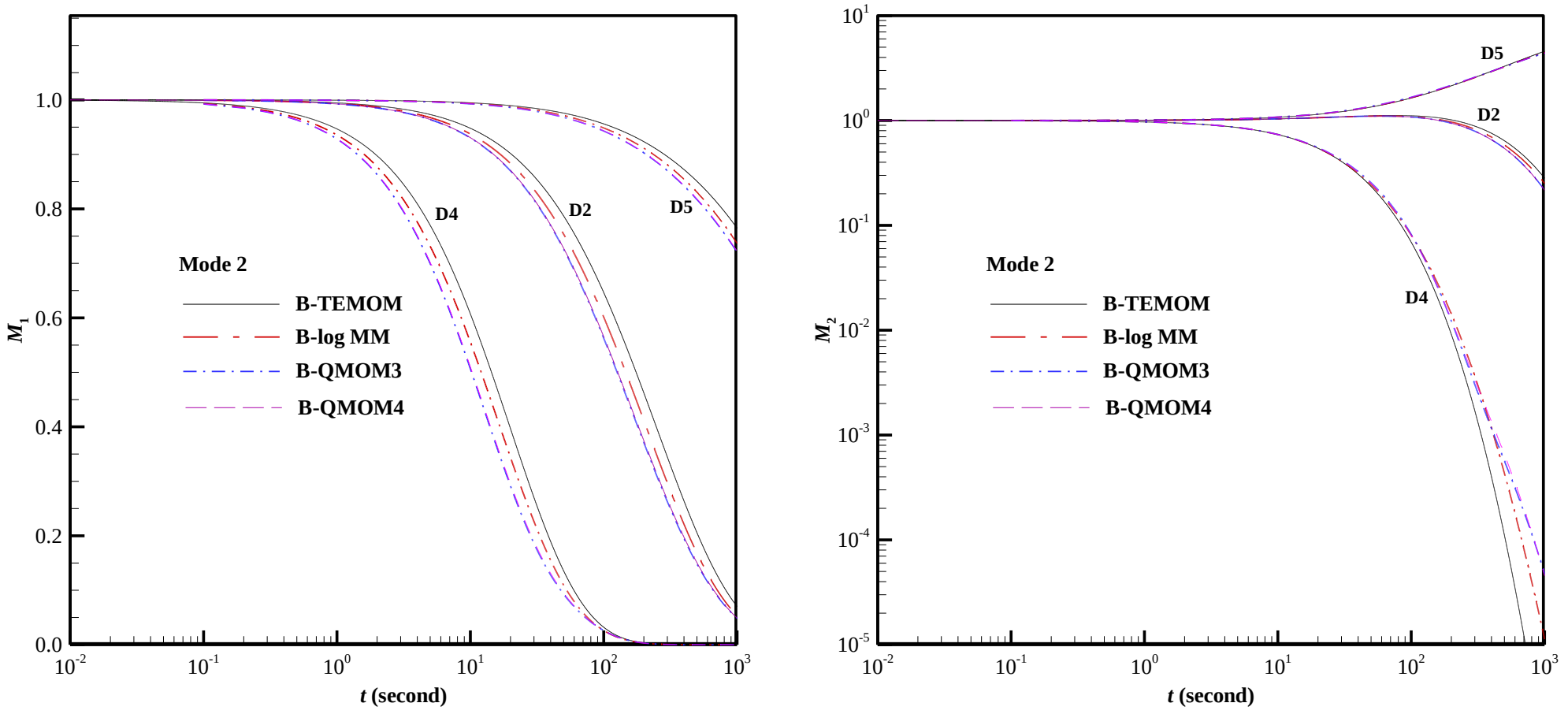

Fig.7 Comparison of dimensionless first and second moments within Mode 2 obtained from B-TEMOM, B-QMOM3, B-QMOM4 and B-log MM models.

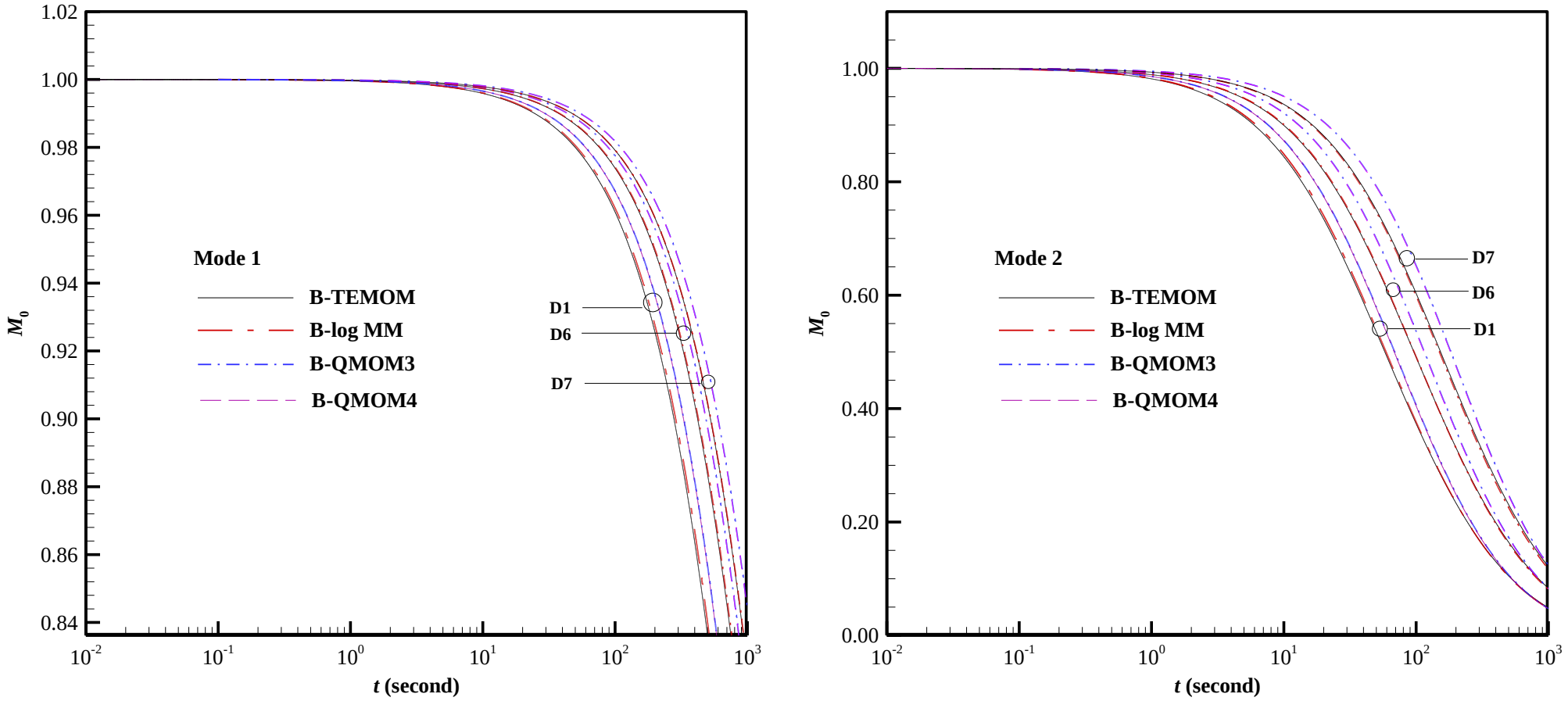

(a) (b)

Fig.8 Comparison of dimensionless zeroth moment of both Mode 1 and Mode 2 obtained from B-TEMOM, B-QMOM3, B-QMOM4 and B-log MM models. $M_0 = \mathrm{m}_0/m_{00}$ for Mode 1, and $M_0 = \mathrm{m}_0/l_{00}$ for Mode 2.

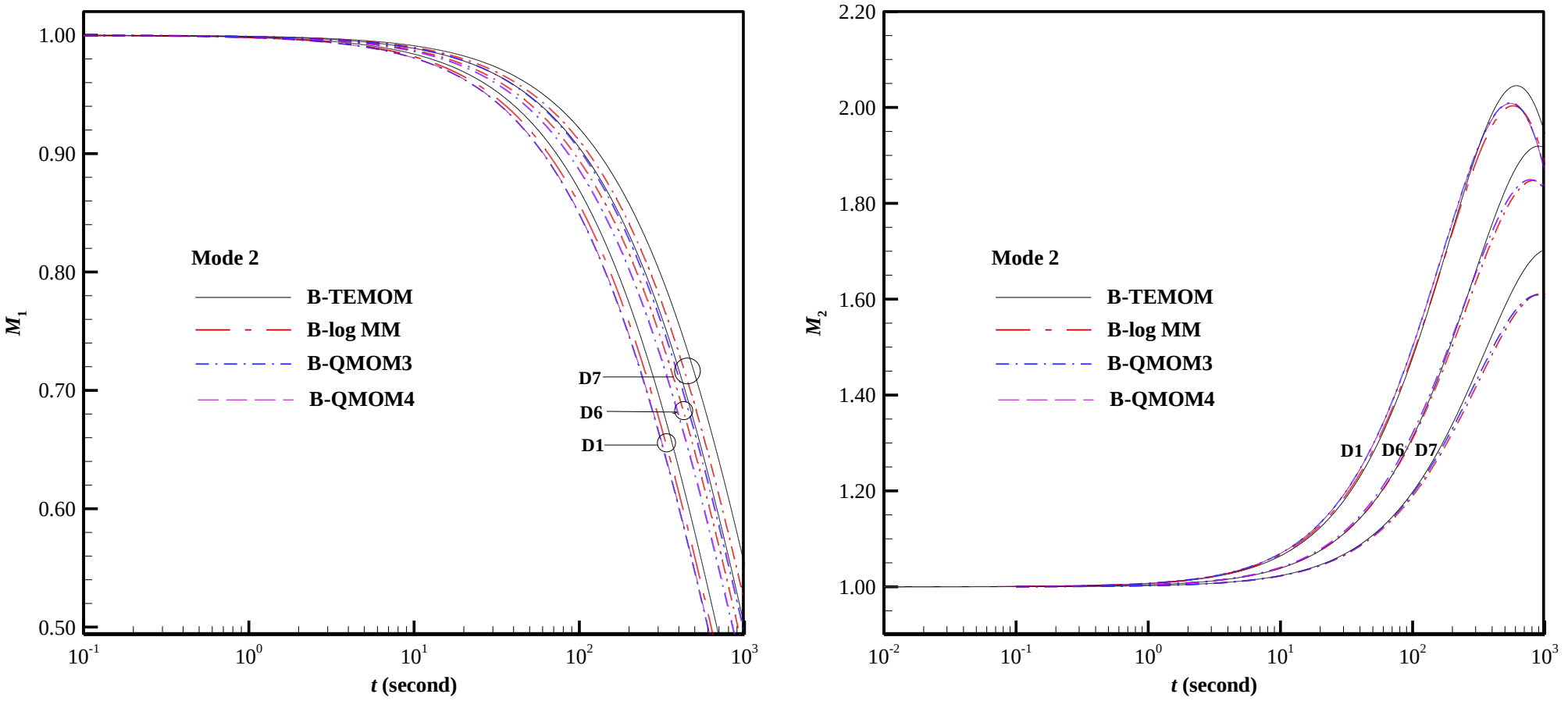

(a) (b)

Fig.9 Comparison of dimensionless first and second moments within Mode 2 obtained from B-TEMOM, B-QMOM3, B-QMOM4 and B-log MM models.

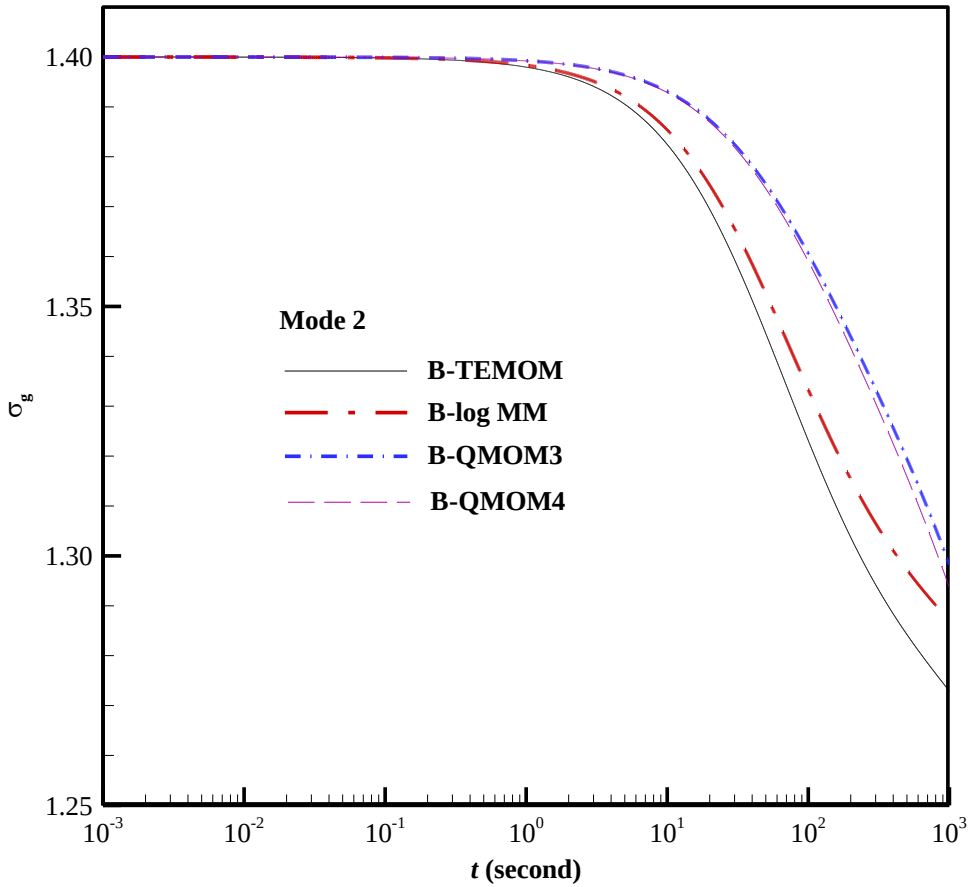

Fig. 10 Comparison of geometric standard deviation with time produced by B-TEMOM, B-log MM and B-QMOM3 (D1) models.

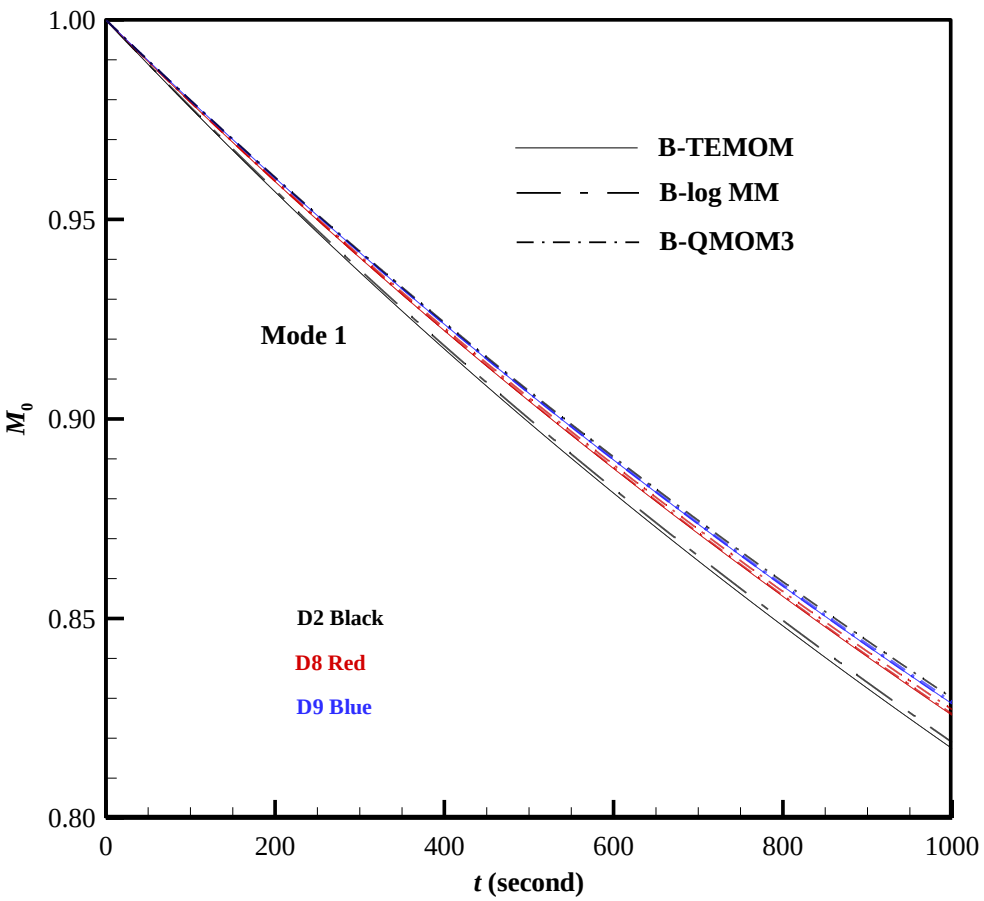

(a)

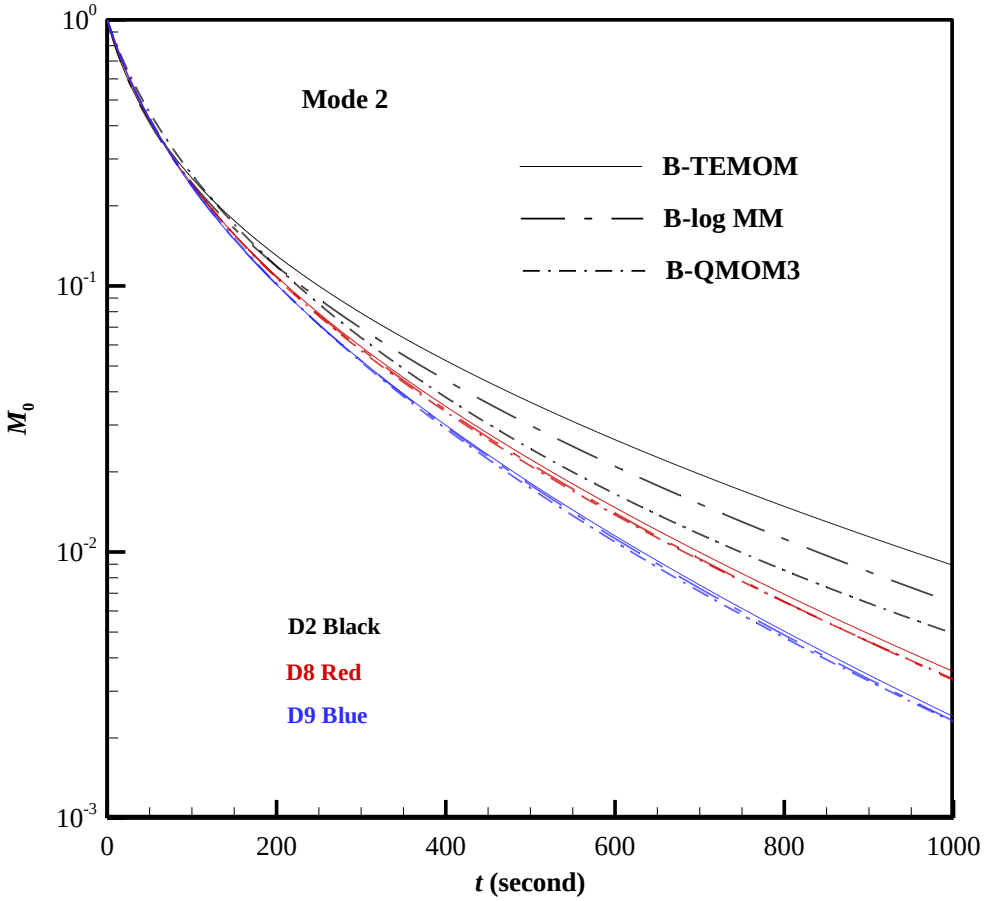

(b)

Fig.11 Comparison of dimensionless zeroth moment of both Mode 1 and Mode 2 obtained from B-TEMOM, B-QMOM3 and B-log MM models. $M_0 = \mathrm{m}_0/m_{00}$ for Mode 1, and $M_0 = \mathrm{m}_0/l_{00}$ for Mode 2.

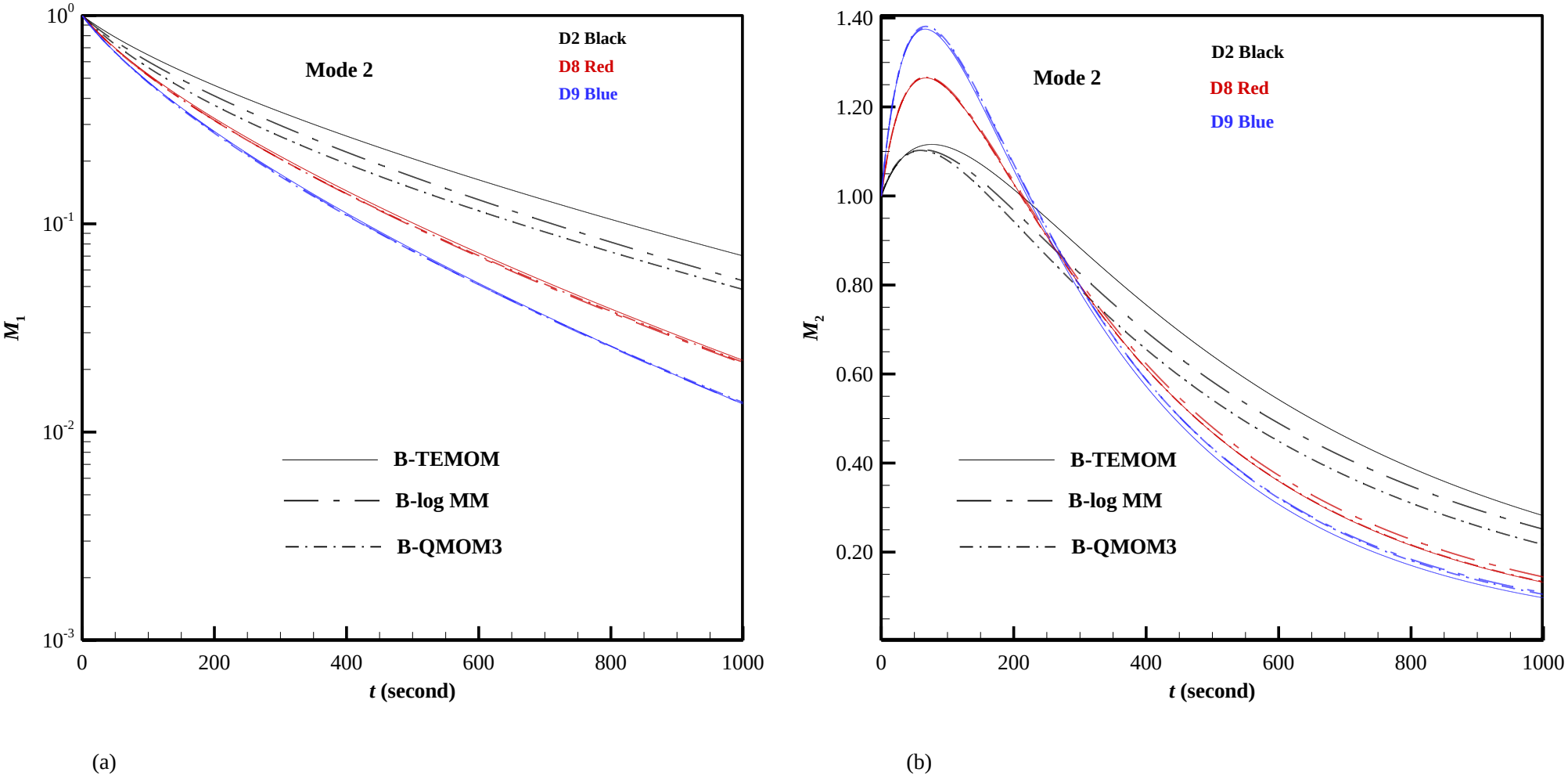

Fig.12 Comparison of dimensionless first and second moments within Mode 2 obtained from B-TEMOM, B-QMOM3 and B-log MM models.